Role of land state in a high resolution mesoscale model for simulating the Uttarakhand heavy rainfall event over India

P V Rajesh, S Pattnaik*, D Rai, K K Osuri, U C Mohanty and S Tripathy

School of Earth, Ocean and Climate Sciences, Indian Institute of Technology Bhubaneswar, Toshali Bhawan, Satya Nagar, Bhubaneswar 751 007, India.
**Corresponding author. e-mail: spt@iitbbs.ac.in*

In 2013, Indian summer monsoon witnessed a very heavy rainfall event (>30 cm/day) over Uttarakhand in north India, claiming more than 5000 lives and property damage worth approximately 40 billion USD. This event was associated with the interaction of two synoptic systems, i.e., intensified subtropical westerly trough over north India and north-westward moving monsoon depression formed over the Bay of Bengal. The event had occurred over highly variable terrain and land surface characteristics. Although global models predicted the large scale event, they failed to predict realistic location, timing, amount, intensity and distribution of rainfall over the region. The goal of this study is to assess the impact of land state conditions in simulating this severe event using a high resolution mesoscale model. The land conditions such as multi-layer soil moisture and soil temperature fields were generated from High Resolution Land Data Assimilation (HRLDAS) modelling system. Two experiments were conducted namely, (1) CNTL (Control, without land data assimilation) and (2) LDAS, with land data assimilation (i.e., with HRLDAS-based soil moisture and temperature fields) using Weather Research and Forecasting (WRF) modelling system. Initial soil moisture correlation and root mean square error for LDAS is 0.73 and 0.05, whereas for CNTL it is 0.63 and 0.053 respectively, with a stronger heat low in LDAS. The differences in wind and moisture transport in LDAS favoured increased moisture transport from Arabian Sea through a convectively unstable region embedded within two low pressure centers over Arabian Sea and Bay of Bengal. The improvement in rainfall is significantly correlated to the persistent generation of potential vorticity (PV) in LDAS. Further, PV tendency analysis confirmed that the increased generation of PV is due to the enhanced horizontal PV advection component rather than the diabatic heating terms due to modified flow fields. These results suggest that, two different synoptic systems merged by the strong interaction of moving PV columns resulted in the strengthening and further amplification of the system over the region in LDAS. This study highlights the importance of better representation of the land surface fields for improved prediction of localized anomalous weather event over India.

1. Introduction

In the year 2013, the Indian summer monsoon (ISM), after a normal onset on 1 June over Kerala, advanced and covered the entire country in a record time (within 15 days), reaching the eastern and the western Himalayan region about a month earlier to its normal date, i.e., 15th July (IMD 2013). Faster advancement of the ISM can be attributed to the northward propagation of the east–west shear zone in the mid-tropospheric levels coupled with convectively active phase of the Madden–Julian Oscillation (MJO) (IMD 2013). A depression was formed over the head of Bay of Bengal (BoB) on 12 UTC

Keywords. Land surface characteristics; high resolution mesoscale model; Uttarakhand rainfall; monsoon season.

J. Earth Syst. Sci. **125**, No. 3, April 2016, pp. 475–498

12 June 2013, which moved northwestward direction and reached north Uttar Pradesh on 12 UTC 17 June 2013 (figure 1a). Simultaneously, a pre-existing westerly trough, while moving eastward, intruded deep into the Indian subcontinent during the same period, eventually interacted with the northwestward moving depression over Uttarakhand and remained stationary for hours. The interaction between these two synoptic scale systems resulted in intensification of the surface low and a strong moisture convergence from the surrounding oceans aided to the heavy orographic lifting over the steep Himalayan terrain (zoomed area shown in figure 1b). This resulted in copious amounts of rainfall and flooding in tributaries of Ganga, inflicting heavy loss to life and property (Kotal *et al.* 2014).

Numerical prediction of heavy rainfall over high and complex terrain under heterogeneous land conditions still remains one of the most challenging tasks for forecasters. Indian subcontinent is geographically diverse, e.g., terrain in the north India ranges up to 6 km (Himalayan region) and it is enclosed by the three major ocean basins on other sides of the country. It is also considered as the major spot where the land–atmosphere is highly coupled and is difficult to model these interactions due to great heterogeneity in soil type, vegetation and terrain (Koster *et al.* 2004). They identified Indian monsoon region amongst one of the globally important locations for feedback between rainfall and soil moisture. Saha *et al.* (2011) also indicated that, post-onset Indian monsoon rainfall variability is greatly determined by the pre-onset land surface conditions and can be improved with the initialization of realistic soil moisture information. However, SM observation network is poor over the region, which hampers the initialization of numerical models, leading to poor performance.

Earlier studies (Trier *et al.* 2004; Holt *et al.* 2005; Lei *et al.* 2008; Chang *et al.* 2009; Kishtawal *et al.* 2010) demonstrated the importance of land surface processes in the evolution of convection events such as monsoon depressions, lows, etc., especially when they are over land. Chang *et al.* (2009) concluded that warmer (cooler) and wetter (drier) land surface can intensify (weaken) the land-falling

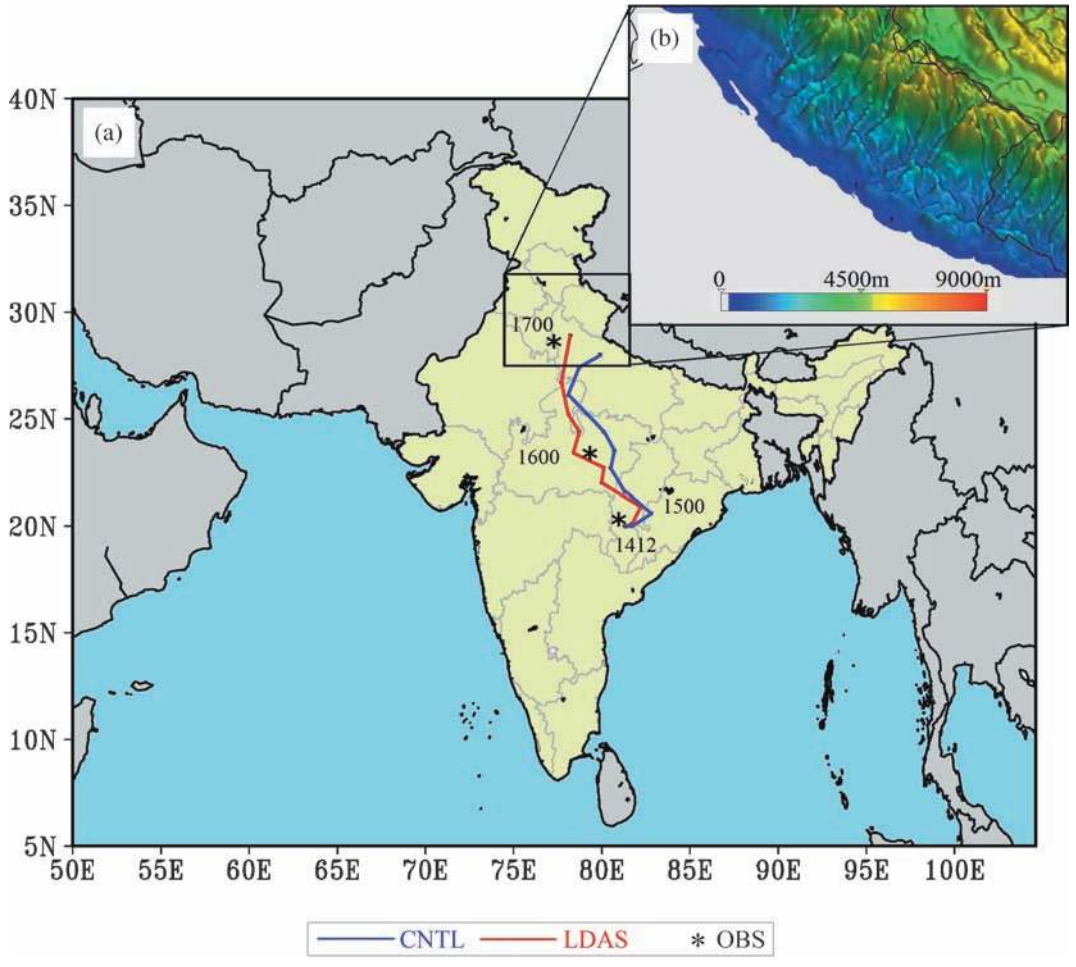

Figure 1. (**a**) Track of the anomalous depression initialized over land, (**b**) red line for the LDAS track and blue line for CNTL. The points represented by 'star' are the locations of the WRF-3DVAR analysis at 00 UTC of 15, 16 and 17 June 2013, respectively. Area enclosed by the box is zoomed out to show the terrain of the heavy rainfall region in inset.

monsoon depressions (MD) over the Indian monsoon region. Vinodkumar *et al.* (2008) showed improved results for a monsoon depression simulation by indirect assimilation of soil moisture (SM) and soil temperature (ST) through flux adjusting surface data assimilation system. Studies over United States have shown a pronounced impact of soil moisture distribution in meridional displacement of storm tracks, which enhances the local soil-moisture-rainfall feedback (Pal *et al.* 2003). This feedback was induced by the local effect of soil moisture in the boundary layer energy budget, which modifies the geopotential height by translating to the large scale.

Chand and Singh (2015) showed that, when the trough of upper troposphere westerlies extends to lower latitudes, it intensifies further by drawing moisture from the Arabian Sea. Mooley (1957) revealed that the early onset (advancement) of monsoon over north and northwest India is associated with an existing western disturbance over the same region. Pisharoty and Desai (1956) and Das (1968) observed the presence of western disturbance over northern India even during the hot summer (April–May). They also documented that the aerial extension of precipitation increases in cases, when a westerly trough interacts with south westerlies from the Arabian Sea or easterlies/south easterlies from the BoB.

Uttarakhand rainfall event was unique, since the interaction of prevailing subtropical westerly flow (trough) during the onset phase of ISM and the line of convergence for these two weather systems nearly remained stationary and virtually locked for hours, resulting in huge amount of rainfall over parts of north India, causing widespread flooding, loss of life and property (IMD 2013). Hara *et al.* (2004), explained undulating upper air westerly flow as potential vorticity oscillation of the relative vorticity caused by the bottom slope. Boos *et al.* (2014) depicted that the monsoon depressions are potential vorticity columns (with peaks in the middle troposphere) that primarily propagate westwards by nonlinear horizontal adiabatic advection, i.e., beta drift. On the other hand, there are studies describing potential vorticity (PV) intrusions from upper to lower levels that move towards lower latitudes during pre-monsoon season over the Indian region (Sandhya and Sridharan 2014). Since the intensification of interacting synoptic disturbances can be better viewed in perspective of PV, diagnosis of PV analysis is carried out based on the potential vorticity tendency equation for a better understanding of interactions between the two systems.

The goal of the present study is to understand the role of high resolution land surface conditions, aiding to the propagation of MD and its dynamic interaction with subtropical upper air westerly flow. Further, it explains the importance of land surface characteristics in improving the simulation of localized rainfall events. Information about the model and datasets are illustrated in section 2. Results and discussions are described in section 3. Finally, the summary of this study is illustrated in section 4.

2. Model and data

2.1 *Modelling system and numerical experiments*

The community HRLDAS is a land data assimilation system based on Noah Land Surface Model (LSM), and is a modelling interface in conjunction with the WRF modelling system. Its dynamical framework calculates temporal changes in surface energy fluxes such as sensible, latent, ground heat fluxes, net radiation, SM, ST, soil water content and surface runoff, etc., in stand-alone (uncoupled) mode. As high resolution SM/ST observations were not available over the region, off-line high resolution SM/ST profiles (with depth) were generated at different soil column layers (0–10 cm, 10–30 cm, 30 cm–1 m, 1–2 m) for parent and nested domains using HRLDAS system (Holt *et al.* 2005; Chen *et al.* 2007). The atmospheric forcing data were obtained from Modern-Era Retrospective Analysis for Research Applications (MERRA) reanalysis at $0.5^\circ \times 0.67^\circ$ resolution in latitude and longitude respectively at 1 hour intervals and these fields were bi-linearly interpolated in space to keep the resolution same in zonal and meridional directions (i.e., $1/2^\circ \times 1/2^\circ$). Rainfall forcing were obtained from tropical rainfall measuring mission (TRMM) 3B42-V7, at 3 hour intervals and with horizontal resolution of $0.25^\circ \times 0.25^\circ$. The initial data to LDAS was derived from Global Land Data Assimilation System (GLDAS) analysis of National Centers for Environmental Prediction (NCEP). The LDAS offline run was carried out for a period of 10 years to ensure a balanced state within the deep soil layers. The model integration duration is from 12 UTC 14 June to 12 UTC 18 June 2013. The detailed information on model configuration and datasets of HRLDAS are provided in table 1.

The Weather Research and Forecasting (WRF) model version 3.6 (Skamarock *et al.* 2008) is used in this study. This model has better skill in capturing different weather phenomena such as heavy rainfall events, monsoon depressions and tropical cyclones (Chen *et al.* 2007; Chang *et al.* 2009). Two experiments were conducted (1) without land data assimilation (i.e., CNTL) and (2) with HRLDAS-based soil moisture and temperature (i.e., LDAS) fields using WRF modelling system. CNTL uses complete atmospheric and land surface fields from

Table 1. *HRLDAS model data details.*

	Source	Horizontal resolution	Temporal resolution
Forcing fields			
Surface pressure (PS)			
2 m temperature (T2)			
2 m mixing ratio (Q2)			
10 m U wind (U10)			
10 m V wind (U10)			
Downward shortwave radiation flux at the surface (SW)	Modern-Era Retrospective Analysis for Research and Applications (MERRA)	0.500 × 0.660	Hourly (from 2003 to 2014)
Downward longwave radiation flux at the surface (LW)			
Rain rate (PCP)	Tropical Rainfall Measuring Mission (TRMM-3B42)	0.250 × 0.250	3 hourly (from 2003 to 2014)
Initialization fields			
ST (at 4 levels)	Global Land Data Assimilation System (GLDAS)	0.250 × 0.250	Initial only
SM (at 4 levels)			
Canopy water content			
Skin temperature			
Water equivalent of accumulated snow depth			
Parametric fields			
Vegetation category	USGS 30-second global 24-category vegetation (land-use)	Interpolated to 4 km	Seasonal/static
Green vegetation fraction			
Minimum and maximum annual green vegetation fraction			
Soil category (at 2 levels)	Hybrid STATSGO/FAO16-category soil texture	Interpolated to 4 km	Static

NCEP Final Analysis (FNL) data. Whereas, LDAS uses atmospheric fields from FNL datasets and surface fields like multilayer SM, ST, canopy water content and skin temperature (Ts) from HRLDAS. Both these experiments were carried out in two-way nested interactive domains having horizontal resolutions of 4 km (inner) and 12 km (parent) with 35 vertical levels and the top of the atmosphere was set at 50 hPa. Surface moisture and temperature fields (SM/ST, skin temperature and canopy water) were updated for both the domains in the LDAS experiment. Both the modelling experiments use Yonsei State University (YSU) planetary boundary layer (PBL) scheme, Monin–Obukhov Janjic surface layer option, RRTM longwave, Goddard shortwave radiation, and WSM6 microphysics with Kain–Fritsch convection for parent domain and explicit convection for inner domain. The performance of high resolutions WRF model (∼4 km) with explicit convection is reasonably good (Done *et al.* 2004). The other land surface characteristics such as vegetation, soil type, land use and land type, etc., were obtained from United States Geological Survey (USGS) data and was kept identical for both the experiments. The complete configuration of the model is provided in table 2.

2.2 *Data*

Surface 2 m temperature and moisture were validated using Global Telecommunication System (GTS) data at 6-hr intervals. Rainfall validation and model skill scores were calculated using IMD daily data at 0.5° × 0.5° resolution (Mitra *et al.* 2013) and time series using TRMM 3B42-V7 (Huffman *et al.* 2007) datasets. Soil moisture verification employs IMD Automatic Weather Station (AWS) data. As track locations for MD is not available, the verification of wind and moisture transport is carried out with analysis prepared using WRF three-dimensional variational (i.e., 3DVAR) analysis by assimilating GTS data using

Table 2. *WRF model configuration.*

Domain and physics	
Grid size (km)	2-way nested:12 km (parent domain), 4 km (inner)
Dimensions (x, y, z)	750 × 500 × 35 (inner)
Time step (s)	20
Model version	3.6
Dynamic core option	Eulerian mass
Microphysics	WSM 6-class graupel (Hong and Lim 2006)
Shortwave radiation	Goddard shortwave ( )
Longwave radiation	RRTM longwave ( )
Surface layer	MM5 Monin–Obukhov (Zhang and Anthes 1982)
Land surface	Unified NOAH land-surface model (Ek 2003)
Boundary layer	Yonsei university (YSU) scheme (Hong *et al.* 2006)
Cumulus	Kain–Fritch (new eta) scheme (Kain 2004)
SST	Fixed (FNL)
Data used	
Initial and boundary conditions	National Centres for Environmental Prediction's (NCEP) FNL data
Resolution	1 × 1, Boundary forcing at 6 hour intervals

FNL fields as first guess. Two-dimensional atmospheric field data from MERRA and TRMM3B42-V7 data were used for forcing HRLDAS and GLDAS datasets for initial conditions. WRF initial and boundary conditions were obtained from FNL datasets.

3. Results and discussion

3.1 *Atmospheric features associated with the rainfall event*

3.1.1 *Surface analysis*

Model-predicted movements of the monsoon depression from CNTL and LDAS experiments are showed in figure 1(a). The zoomed area within the rectangular box (figure 1a) shows the terrain (figure 1b) of the heavy rainfall region. As the minimum sea level pressure (MSLP) was spread over a large area, 850 hPa wind flow pattern vortex center is used to locate the depression center that formed over northwest BoB and moved from 12 UTC 14 June till 00 UTC 17 June 2013 at 3-hr intervals. The center points obtained from 3DVAR analysis (showed as 'star' sign) at 12 UTC 14, 00 UTC of 15, 16 and 17 June is used to verify the model-predicted MD locations for the same period. There is a rightward bias in the CNTL track, whereas, the LDAS track is improved considerably with the availability of realistic land surface conditions with respect to WRF-3DVAR (observation) locations. The improvement in track movement valid for 00 UTC 15 June from LDAS is 35 km, which is further increased to 197 km valid for 00 UTC 17 June forecast. It was noted that the land surface is more moist in LDAS-based initial conditions than that of CNTL over central and north western regions (figure 2). Figure 2 also shows the spatial distribution of initial values of top layers (i.e., 0–10 cm) SM in $m^3\ m^{-3}$ (figure 2a and b); and ST (figure 2c and d) in K for CNTL and LDAS experiments. From TRMM observations, during 13–14 June, light rainfall had occurred over northern India and moderate-to-heavy rainfall over the central India (not shown). The CNTL-based initial conditions show comparatively drier and hotter along the monsoon trough region, which does not reflect the changes of land surface with the prior rainfall associated with the monsoon depression. LDAS-based SM shows comparatively wetter soil (0.2–0.25 $m^3\ m^{-3}$) along the monsoon trough region showing response with the previous day rainfall. Earlier studies demonstrated that prior wetter conditions had resulted in improved inland movement of the depressions (Ashu Dastoor and Krishnamurti 1991; Chang *et al.* 2009; Yoon and Huang 2012). LDAS-based ST distribution shows stronger heat low over northwestern parts of the Indian subcontinent (>320 K), Arabian Desert and a warm Tibetan Plateau.

The SM verification results from both experiments for 72-hr forecast with IMD AWS observations at available (299) stations within the entire domain are presented in figure 3. The correlation coefficient for CNTL and LDAS are 0.63 and 0.73, while root mean square errors (RMSE) are 0.056 and 0.05, respectively. Note that the CNTL-simulated SM showed overestimation (underestimation) for smaller (higher) values, while the LDAS provided consistent SM values over India, though there is a spread which is marginal. From this, it is obvious that the high resolution SM

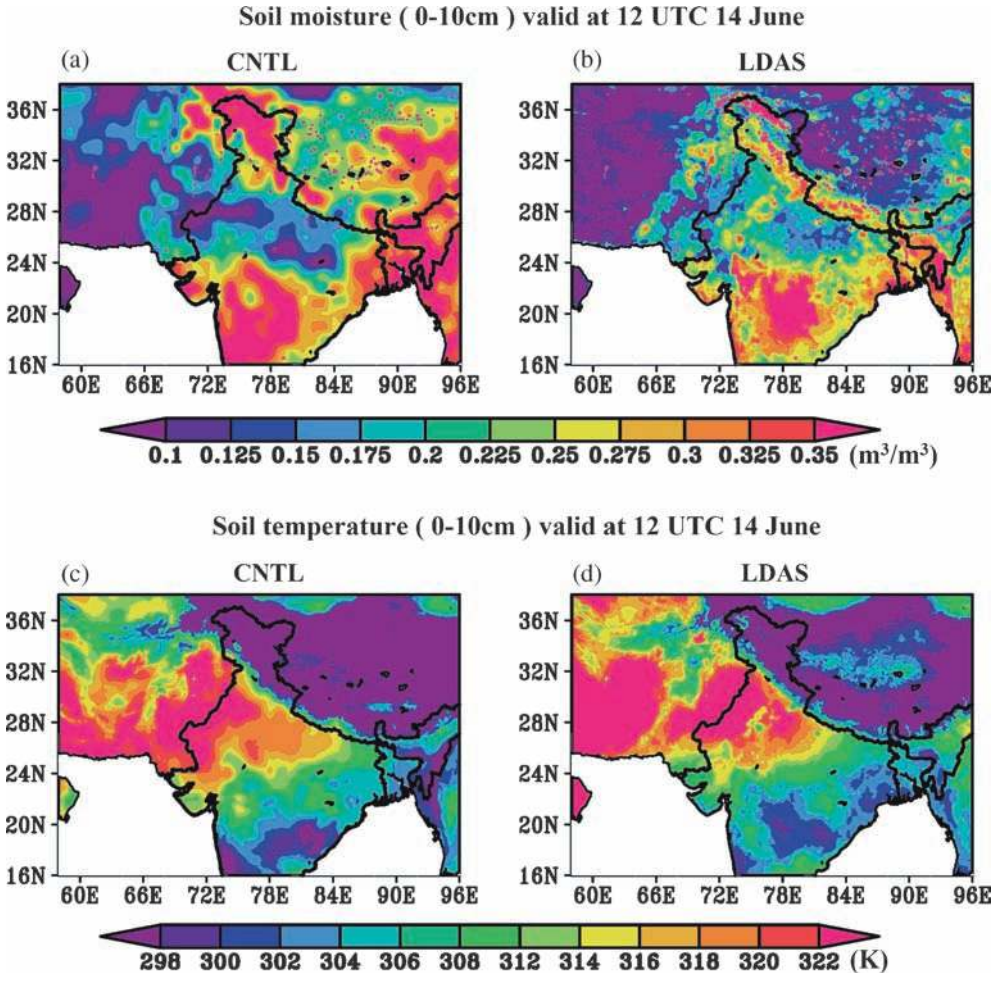

Figure 2. (**a** and **b**) Distribution of initial soil moisture (m^3m^{-3}) and (**c** and **d**) soil temperature (K) for CNTL and LDAS for parent domain (12 km).

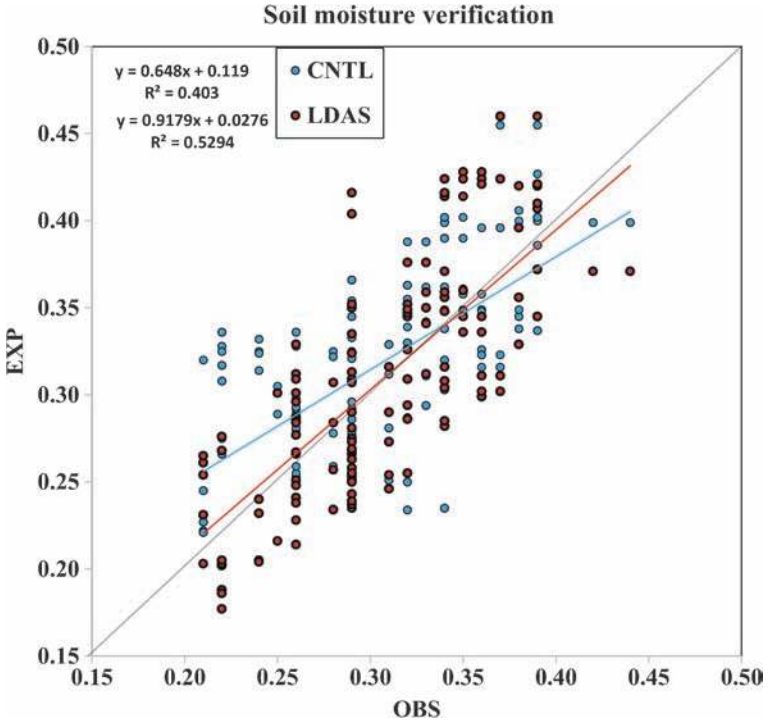

Figure 3. Scatter plot of IMD, AWS soil moisture data against CNTL and LDAS for the 72-hr simulation period.

obtained from assimilation used in LDAS were able to capture the grid point scale variability. The intercept theoretically should be 0, whereas for LDAS and CNTL it was found to be 0.03 and 0.12, respectively. The initial SM (i.e., 12 UTC 14 June 2013) used in CNTL obtained from GDAS, was found to have a wet bias below 0.32, and dry bias above with 26° slope. In the case of LDAS, the wet bias is below 0.21 and dry bias above with slope of 35° (figure not shown). Thus it is clear that LDAS could represent better SM conditions than CNTL throughout the simulation duration in terms of variability and range. Figure 4 shows difference (LDAS minus CNTL) of latent and sensible heat fluxes valid for 24 and 48 hr forecast. It is observed that the difference in sensible heat flux between LDAS and CNTL is between −60 and 60 W m^{-2}, except over the Tibetan Plateau (figure 4b). Enhanced latent heat flux (50–100 W m^{-2}) was noticed over central and northwestern India in LDAS (figure 4a), which can be attributed to the enhanced soil moisture over the same region (figure 2b).

Figure 5 shows correlation and RMSE of simulated 2 m temperature (T2) and relative humidity (RH2) with respect to available GTS observations within the entire forecast duration (∼341–390 locations), at every 6-hr intervals. Throughout the integration, LDAS correlation coefficient for RH is high compared to CNTL, except initial hours (i.e., 0∼6 hr) inferring an improved heterogeneity in SM simulated by the LDAS. While, the same is lesser in CNTL, which utilizes coarser resolution Global Data Assimilation System (GDAS) SM in the model (figure 5a). The RMSEs of both the variables are less in LDAS. The T2 correlation is stronger in daytime than night time, suggests a better representation of evolution of daytime Planetary Boundary Layer (PBL). It is noted that initial 6-hr forecast does not show any difference between CNTL and LDAS, which can be attributed to the spin up of the model. However, during 12–72 hr of model integration, the RH2 and T2 RMSE in LDAS is reduced to a minimum (21% and 4 K) at 60-hr forecast (i.e., 00 UTC 17 June), while significant improvement in LDAS over CNTL is observed at 48-hr forecast, 12 hr prior (i.e., 12 UTC 16 June) for RH2 and T2 in terms of correlation and RMSE.

3.1.2 *Wind and moisture transport*

Figure 6 shows the vertically integrated moisture transport and 850 hPa wind vector from LDAS

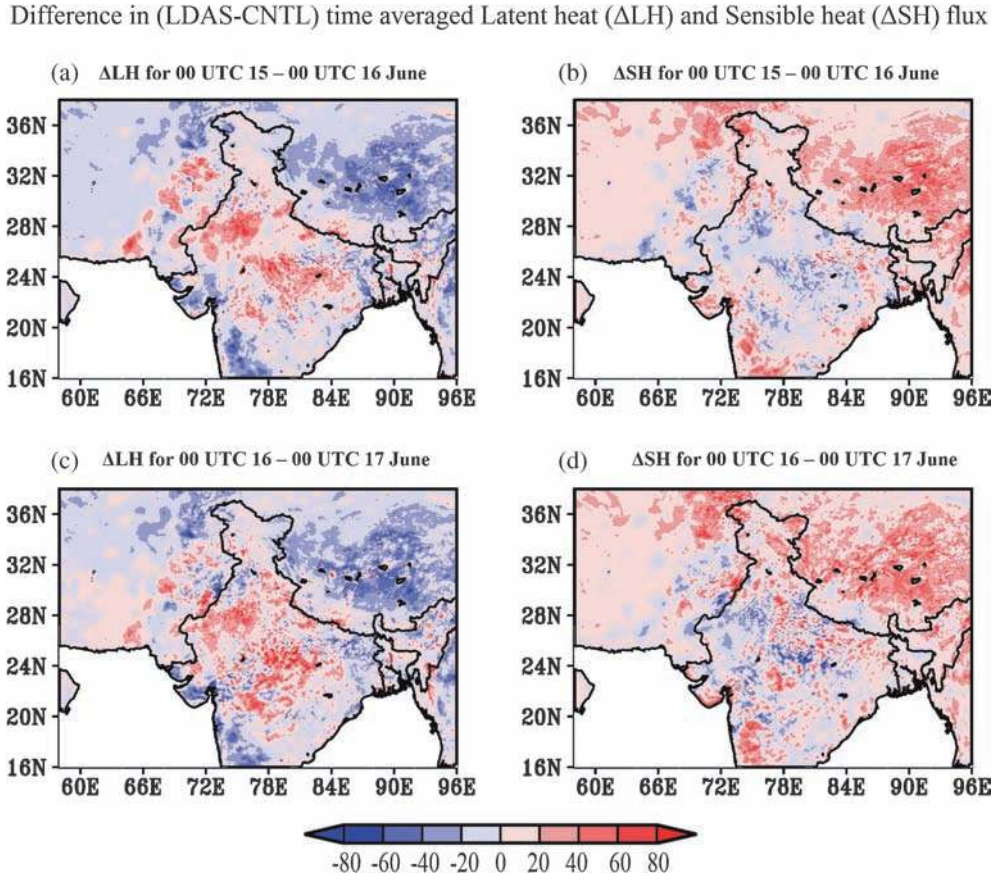

Figure 4. Difference in time averaged sensible heat (ΔSH), latent heat flux (ΔLH) in W m^{-2} between LDAS and CNTL for 00 UTC 15 June–00 UTC 16 June (**a** and **c**), for 00 UTC 16 June–00 UTC 17 June (**b** and **d**).

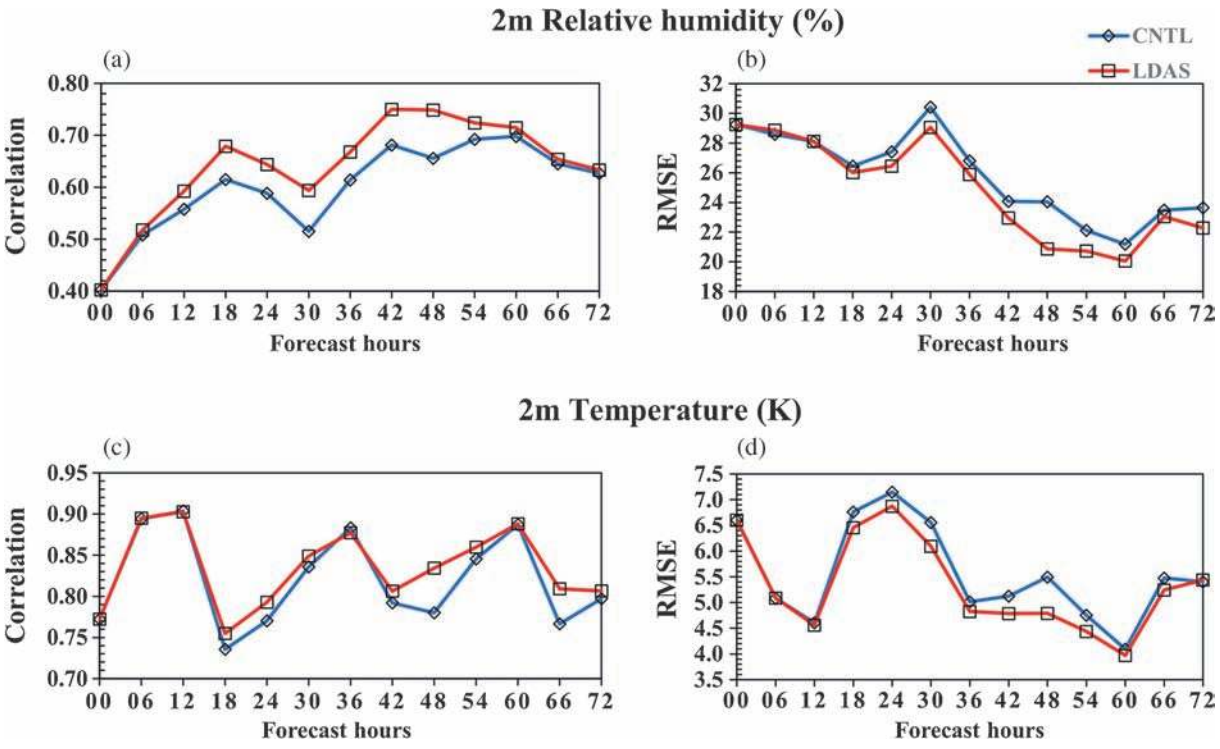

Figure 5. (**a**–**b**) Verification of model-simulated correlation coefficient and RMSE of relative humidity (%), (**c**–**d**) 2 m temperature (K) for CNTL and LDAS simulations respectively, with available synoptic point observations within the domain.

(figure 6b, e, h, k, 2nd column), WRF-3dvar analysis (figure 6a, d, g, j, 1st column) and the difference (i.e., LDAS – CNTL) at 00 UTC of 15, 16, 17 and 18 June 2013, respectively. It is evident that there are two low pressure systems, one depression is around 81.6°E, 20.0°N with well-marked cyclonic circulation covering entire Indian subcontinent and vertically extended up to 250 mb, and another low pressure area over Arabian Sea (66.7°E, 21.1°N), in which the cyclonic circulation extended up to 500 mb (figure 6a). The vertically integrated moisture transport through the entire atmospheric column shows intense moisture transport (300∼400 kg ms^{-1}) from Arabian Sea and BoB into system lies at 80°E and 20°N (figure 6a). The simulated wind field and moisture transport in LDAS are close to the WRF-3dvar analyses at 00 UTC of 15 June. The difference in the moisture transport between LDAS and CNTL is less (<100 kg ms^{-1}) in 12 hr of forecast, particularly over the central India. However, LDAS shows relatively higher moisture transport from the vicinity of Arabian Sea and BoB systems by about 150∼200 kg $m^{-1}s^{-1}$, particularly for forecast valid for 00 UTC 17 June, as compared to CNTL (figure 6c).

The position and strength of the monsoon flow in LDAS is in good agreement with 3DVAR analysis (figure 6a, b, d, e, g, h). The location of monsoon depression is also well simulated by LDAS (76°E, 24°N) compared to CNTL. The LDAS shows relatively stronger westerlies of the order 10–20 ms^{-1} from the Arabian Sea (figure 6b, e, h). At 00 UTC of 17 June, after the monsoon depression was merged with the monsoon trough and the resultant system with intense moisture transport (>800 kg $m^{-1}s^{-1}$) was moved northern latitudes towards Uttarakhand region (figure 6h).

To get a broad picture of the moisture transport prior to the heavy rainfall event, daily averaged difference (LDAS–CNTL) of vertically integrated moisture transport and 850 hPa wind speed from 00 UTC 15–00 UTC 16 June and 00 UTC 16–00 UTC 17 June are computed. A distinct narrow channel of moisture anomaly from Arabian Sea with two distinct anomalous circulations on either side (figure 7b) is observed. To the left side, a cyclonic circulation and to right an anticyclonic anomaly is visible and the convergence boundary of the two circulations is subjected to large wind speed anomaly (∼8 ms^{-1}) and moisture transport. The stronger anomalous cyclonic circulation in LDAS seems to bring the excess moisture from Arabian Sea in LDAS and this resulted in the rainfall event at 00 UTC 17 June.

To see land surface feedbacks for abundant moisture transport into the heavy rainfall region of Uttarakhand in case of LDAS, difference between SM, ST and vertical velocity between LDAS and CNTL averaged from 12 UTC of 16 to 00 UTC 17 June are computed. The result shows (figure 8a),

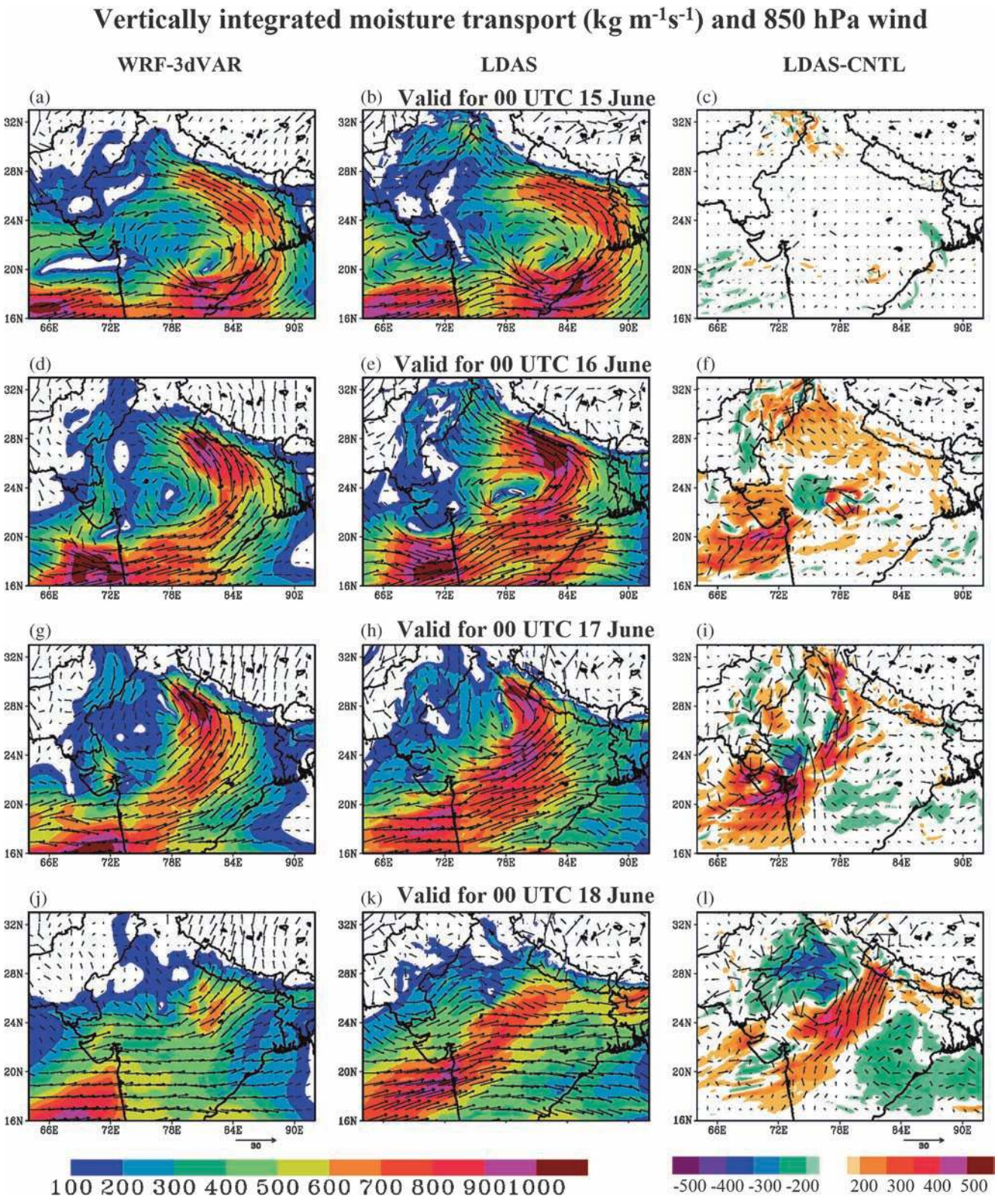

Figure 6. (**a**, **d**, **g**, **j**) Vertically integrated moisture transport (kg $m^{-1}s^{-1}$) (shaded) and 850 hPa wind vector of WRF-3DVAR analysis, (**b, e, h, k**) LDAS and (**c**, **f**, **i**, **l**) difference (LDAS-CNTL) for outer domain validated at 00 UTC of 15, 16, 17 and 18 June 2013.

a distinct narrow drier region embedded inbetween relatively wet regions with stronger gradients on either sides, extended linearly about 8° into the vicinity of the affected area. Soil temperature distribution (figure 8a) also shows an elongated region of warmer soil over the same location. Recent study

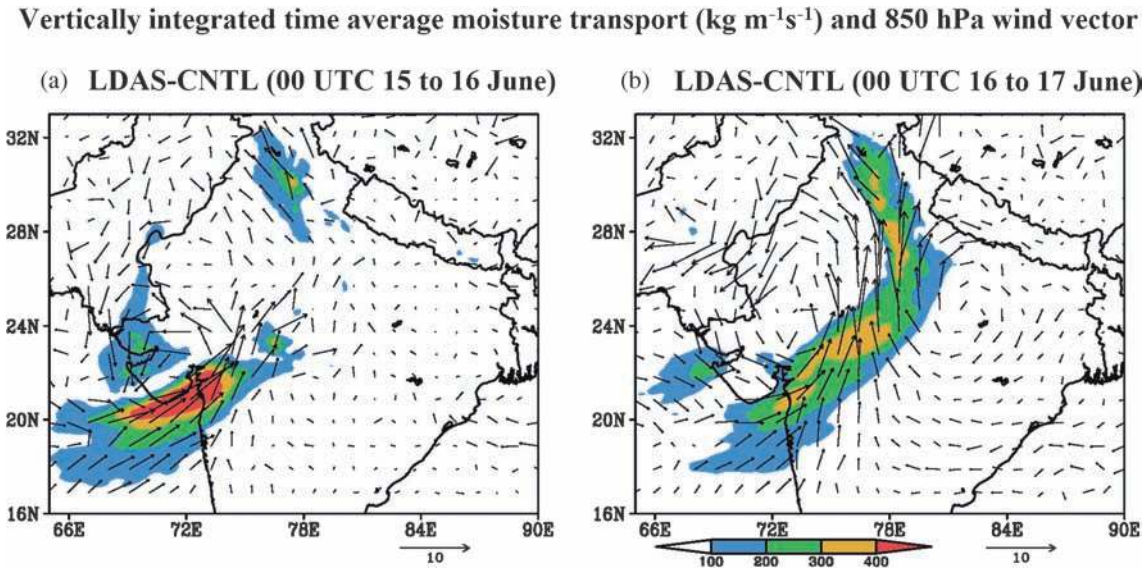

Figure 7. Difference between LDAS and CNTL (LDAS-CNTL) vertically integrated moisture transport (kg $m^{-1}s^{-1}$) and 850 hPa wind vector averaged (**a**) for 00 UTC 15 June to 00 UTC 16 June and (**b**) for 00 UTC 16 June to 00 UTC 17 June 2013.

(Guillod *et al.* 2015) suggests that the contrast in soil conditions, especially SM will induce local circulations and can generate vertical motions along the regions of strong discontinuity in SM. The LDAS produced strong updrafts (figure 8c) than CNTL over the region and is consistent with the findings of Guillod *et al.* (2015), suggesting that a relatively strong convective region exists in LDAS compared to CNTL, along the line of strong SM gradients. In nutshell, it is clear that though both the experiments could reproduce the observed synoptic features, LDAS was able to reproduce the improved moisture transport from Arabian Sea in this particular event, facilitated by the improved representation of land surface features. It is also clear that though monsoon current drew-in moisture both from the Arabian Sea and BoB during 15–16 June and afterwards, the moisture incursion was dominant from Arabian Sea, which is in agreement with the synoptic features observed by IMD (IMD 2013).

Figure 9(a and b) represents the terrain along east–west direction and vectors represent the zonal winds (vertical velocity is magnified to an order of 10) and shaded represents the meridional winds for CNTL and LDAS, respectively. Figure 9(b and c) are same but along zonal direction. Vertical distribution of wind vectors at 18 UTC 16 June shows stronger orographic lifting (figure 9) in LDAS compared to CNTL. The contribution of orographic lifting in LDAS is distinct over the location marked by the black elliptical region in figure 9(b and d).

Figure 10(a) shows the time averaged (i.e., 00 UTC 16 June–00 UTC 17 June) Convective Available Potential Energy (CAPE) and the difference (LDAS–CNTL). Stronger band of CAPE is observed (>400 J kg^{-1}) across the central-eastern parts extending towards the northern India. It is to be noted that the eastern parts of Uttarakhand show a pocket of comparatively less CAPE with respect to CNTL. The temporal evolution shows (figure 10c) an increase in CAPE after 00 UTC 16 June and peak at 12 UTC 16 June, thereafter a reduction in magnitude in both the experiments, in which LDAS shows an increased CAPE of more than 100 J/kg with respect to CNTL for this period. The contribution from CAPE is clearly visible from the Skew-T diagram calculated at (79°E, 30°N) at 12 UTC 16 June (figure 10c). LDAS shows stronger CAPE (4201 J kg^{-1}) and strong Lifted Index (−9 K), with larger dew point depression in the upper levels compared to CNTL (figure 10d). The stronger instability in LDAS experiment can be attributed for the intensification of the surface low centered over Uttarakhand.

The upper air westerlies at 200 mb from the WRF-3DVAR analysis and the model simulations made clear that both the experiments (i.e., CNTL and LDAS) were able to capture the flow close to the 3DVAR analysis. However, the differences in the upper air wind flow between CNTL and LDAS are less throughout the simulation period (figure not shown). The trough line stayed northwest of Jammu and Kashmir, passing through Pakistan as observed on 15 June, which subsequently intensified and intruded southwards on 00 UTC of 17 June. Wind speeds exceeding 100 m s^{-1} (jet streak) is observed in the eastern side of the upper air trough (>36°N and >78°E) at 00 UTC 16 June, that leads to the further intensification of the westerly trough. The low level jet (LLJ) also appears

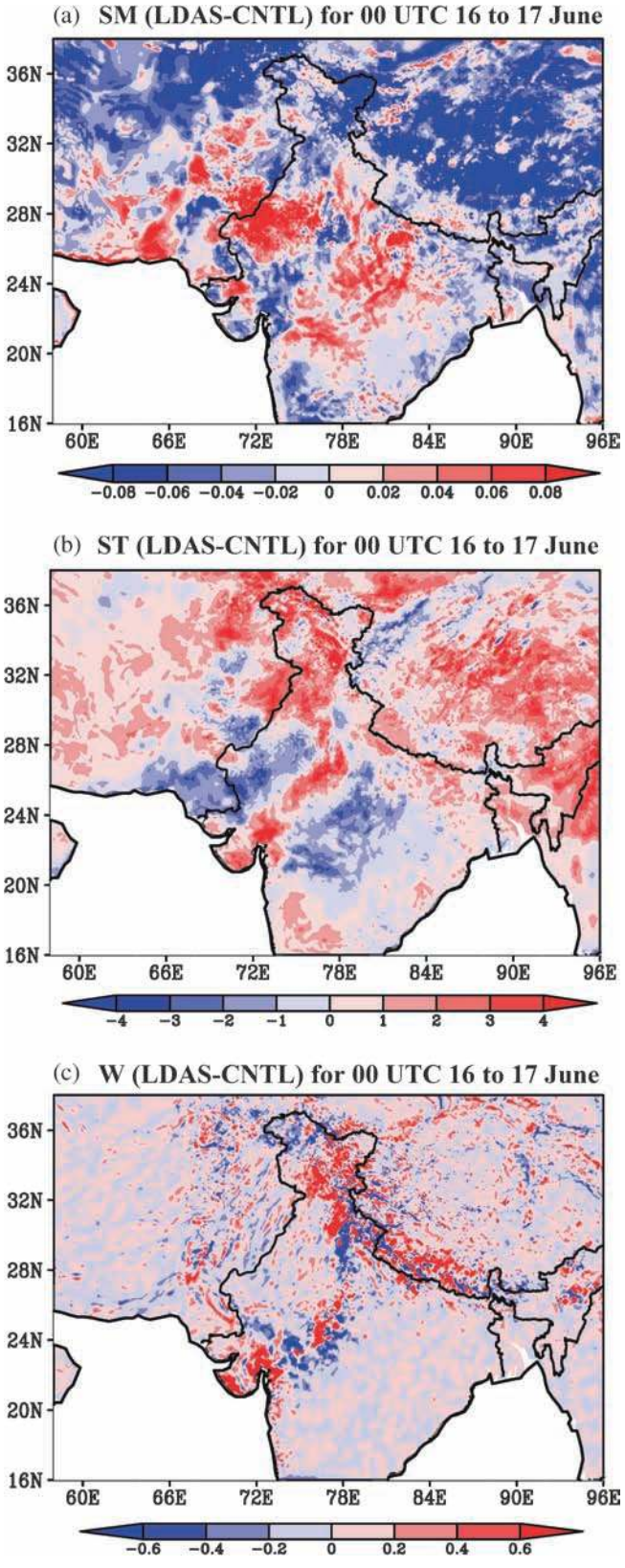

Figure 8. Difference between LDAS and CNTL (LDAS-CNTL) for 00 UTC 16–00 UTC 17 June 2013 (**a**) SM ($m^3\ m^{-3}$), (**b**) ST (K) and (**c**) vertical velocity W ($m\ s^{-1}$).

active and coupling of westerly trough induced surface low over northern India could have helped the accelerated movement of monsoonal system by facilitating the mechanism of low level moisture convergence from both the surrounding seas, deep into the mainland.

3.1.3 *Rainfall*

Daily accumulated rainfall comparison between model simulations and IMD data at 0.5° × 0.5° resolution (Mitra *et al.* 2013) are shown in figure 11(a–i). The heavy rainfall region from IMD data is identified within the region bounded by 78°–80°E, 29°–31°N and is selected for latter diagnosis. The observed station rainfall distribution indicates that heavy rainfall (>100 mm) occurred on 16 and 17 June 2013 over the western districts of Uttarakhand, thereafter shifting eastward across Uttarakhand. The rainfall valid for 16 June is underestimated by both CNTL and LDAS (∼30–60 mm) and both these experiments show nearly same rainfall distribution (figure 11a–c). For the rainfall valid on 00 UTC 17 June, CNTL and LDAS show reasonable spatial distribution rainfall amounts with respect to IMD observations, but there is a considerable improvement in the location and amount of rainfall in LDAS with respect to CNTL over the northern parts, especially in simulating the elongated band of rainfall centered at 30°–78°N (figure 11f). This heavy rainfall band in LDAS is well explained by the occurrence of high moisture transport from Arabian Sea (figure 7b). Results valid for 00 UTC 18 June shows a southeastward shift with narrowed and confined rainfall region in the LDAS (figure 11i) in contrast to dispersed rainfall in the CNTL. Based on IMD data, heavy rainfall region for the entire episode is located within the 77°–81°E, 28°–31.5°N.

Figure 10(c) shows the time series of area averaged (3-hourly accumulated) rainfall over the same region as shown in figure 11, along with the deep layer (850–300 hPa) vertical velocities ($hPa\ s^{-1}$) in 3-hr intervals. The corresponding TRMM rainfall was not able to capture the rainfall peaks between 00 UTC and 18 UTC 17 June and underestimated the amount and intensity of rainfall. Comparison of 24-hr accumulated rainfall averaged over the same region obtained from IMD observations and TRMM, shows that TRMM underestimated the peak rainfall by about 112 mm (figure not shown).

The model skill in predicting of daily rainfall is investigated by calculating the Equitable Threat Scores (ETS), Probability of Detection (POD) and False Alarm Ratio (FAR) for different thresholds by using IMD daily rainfall observations. The ETS is based on the Critical Success Index (CSI), corrected for the number of hits that would be expected by chance. ETS ranges from 0 to 1 and

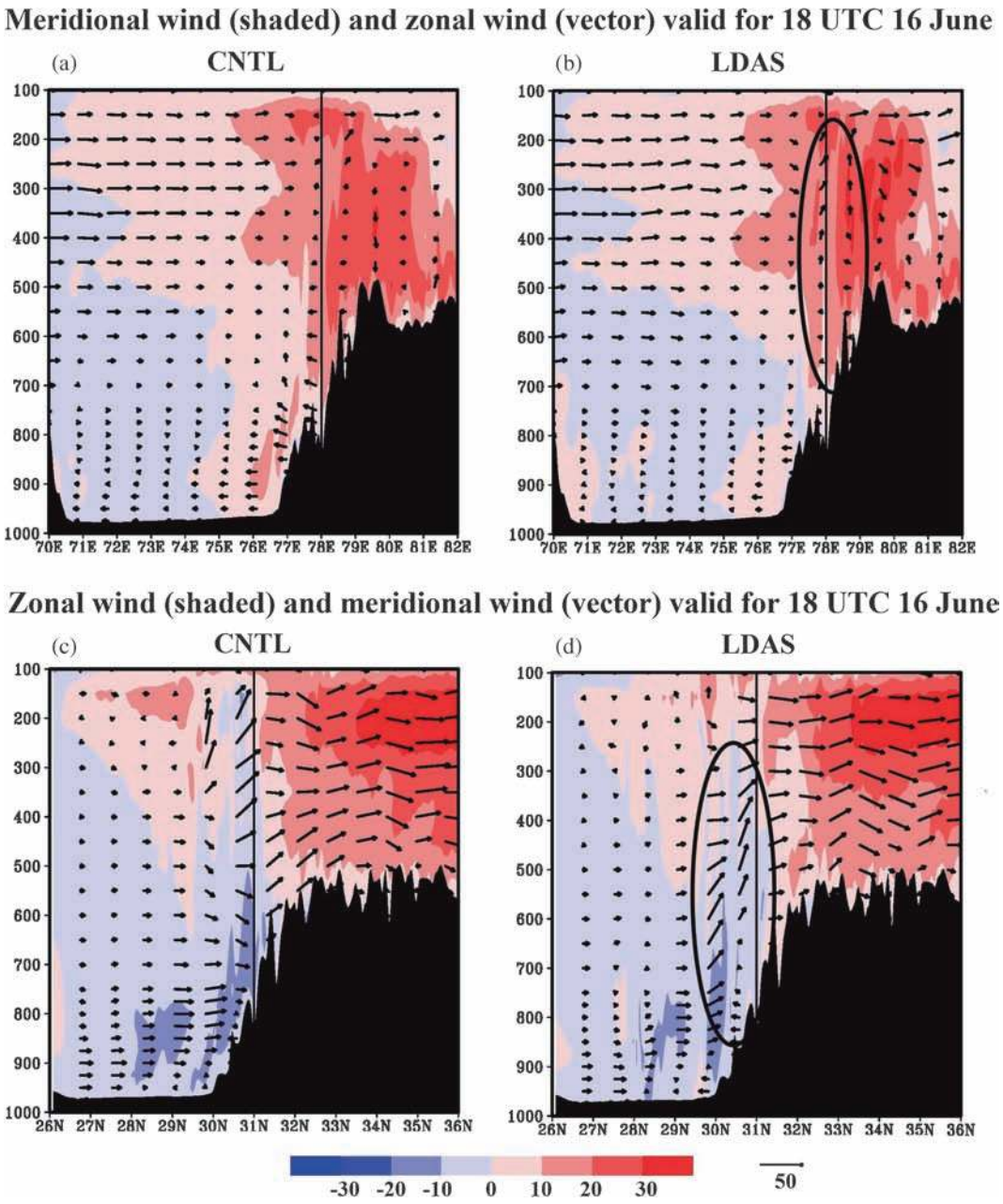

Figure 9. Vertical cross-section of wind zonal (vector) and meridional (shaded) for CNTL and LDAS viewed across longitude (**a**–**b**), and viewed across latitude (**c**–**d**). The vertical black line shows the center of heavy rainfall region and region of high orographic vertical upliftment in LDAS is highlighted using the thick black elliptic. Vertical velocity is magnified to an order of 10.

perfect forecast would have ETS = 1. POD is the fraction of events that were correctly forecasted to occur; it ranges from 0 to 1 and POD = 1 implies perfect forecast. FAR is the proportion of forecasts of the event occurring for which the event did not occur. FAR ranges from 0 to 1 and for a perfect forecast FAR = 0. The LDAS showed improved ETS, POD and FAR for moderate rainfall valid for 16 June 2013 for all the thresholds up to 80 mm (figure 12a, d, g), though both the experiments underestimates the rainfall amount. The correlation, RMSE, mean error and multiplicative bias for CNTL/LDAS are respectively 0.27/0.35, 80/73 mm, −49/−35 mm and 0.21/0.29. The credibility of LDAS can be seen during the very heavy rainfall days (17–18 June 2013). It had predicted very heavy rainfall up to 200 mm (figure 12b, e, h) with maximum ETS reaching up to 0.22 for 00 UTC 17 June with marginal increase in POD and reduction of FAR for the entire threshold spectrum. For this duration, correlation, RMSE, mean error and multiplicative bias for CNTL and LDAS are respectively 0.53/0.64, 112/97 mm, –68/–53 mm and 0.37/0.43.

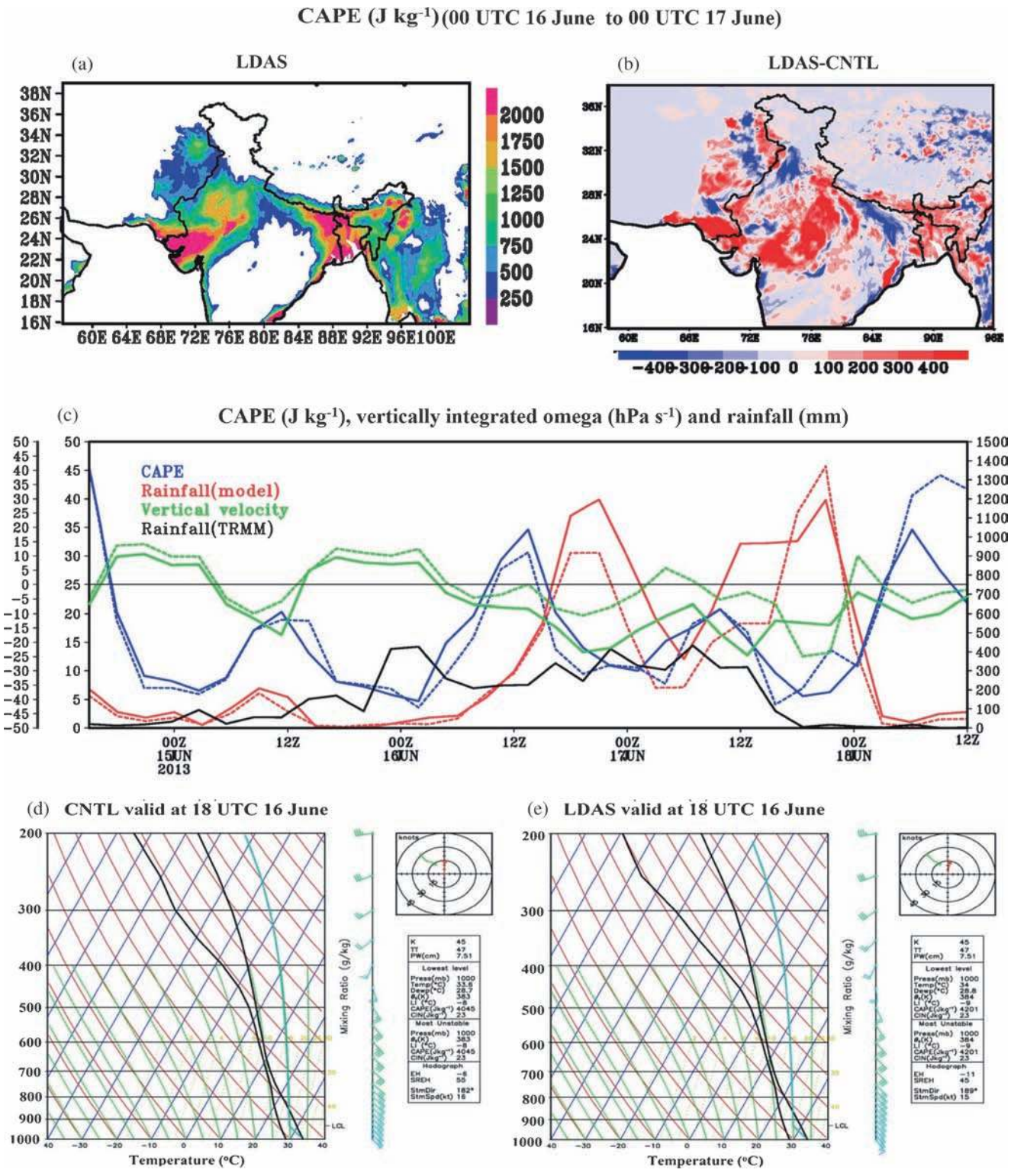

Figure 10. (**a**) Averaged (00 UTC 16 June to 00 UTC 17 June) Convective Available Potential Energy (CAPE) (J kg^{-1}) and (**b**) the difference in CAPE between LDAS and CNTL for the same duration, (**c**) temporal evolution of CAPE (blue), averaged vertical velocity omega (hPa s^{-1}) (green), model rainfall (mm), (red) along with TRMM rainfall (black). Skew-T diagram averaged for the heavy rainfall region, (**d**) for CNTL and (**e**) for LDAS respectively. All the fields are area averaged over the heavy rainfall region shown with LDAS (line) and CNTL (dotted).

Rainfall statistics for 18 June have the maximum impact in LDAS by capturing the rainfall with ETS greater than 0.29 and similar improvement is observed detecting the rainfall amounts with least error in terms of POD and FAR (figure 12c, f, i). While, for the same threshold, CNTL predicted

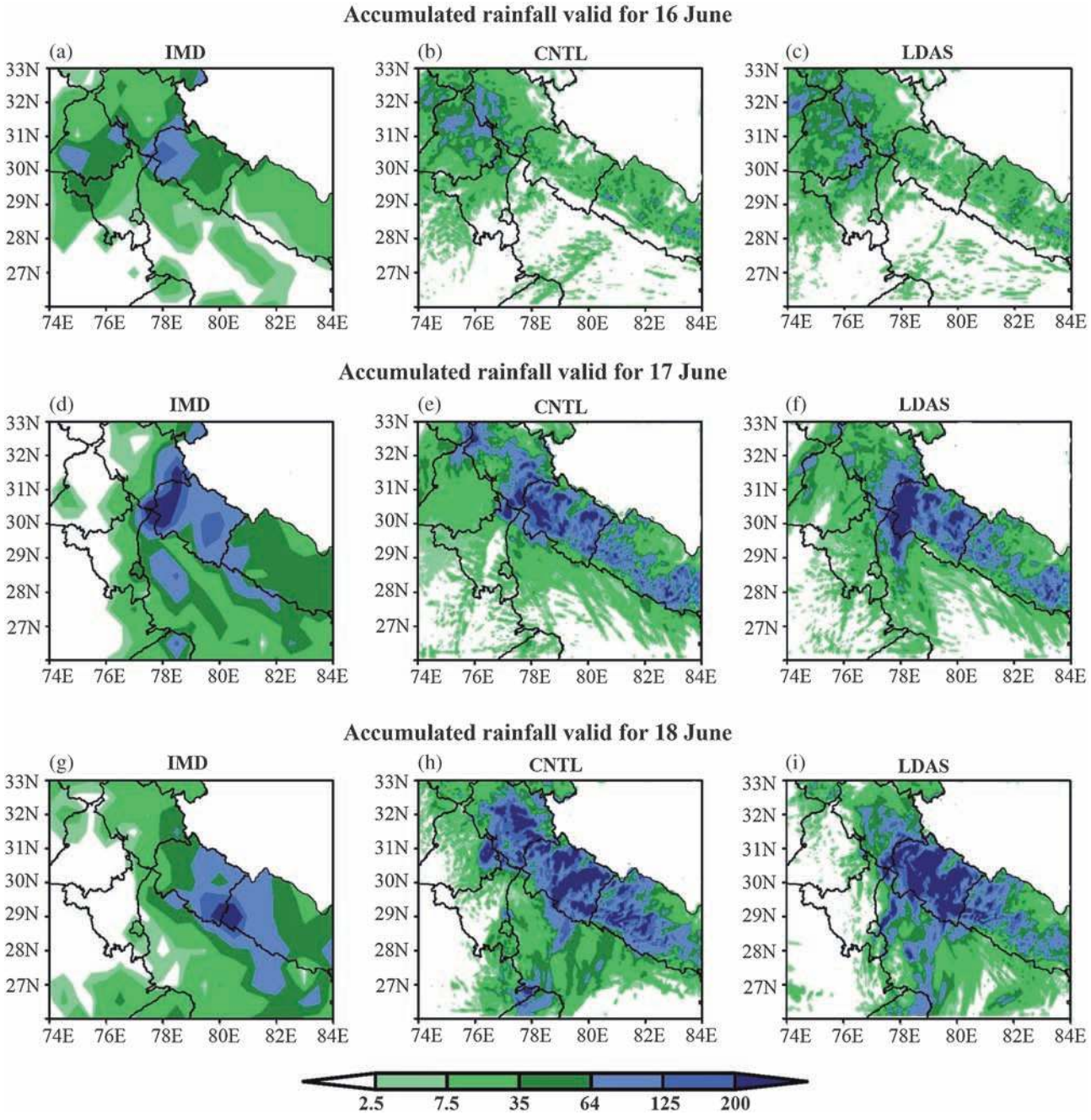

Figure 11. (**b**, **e**, **h**) Daily accumulated rainfall (mm) for CNTL (**c**, **f**, **i**), LDAS (**c**, **f**, **i**), IMD (**a**, **d**, **g**) valid for 16, 17 and 18 June 2013.

with relatively less ETS, with maximum up to 0.18 and 0.2 respectively, for the same period. The correlation, RMSE, mean error and multiplicative bias for 18 June CNTL/LDAS are respectively 0.37/0.47, 115/94 mm, –10/–4 mm and 0.80/0.90. It is found that, in general, LDAS consistently shows better rainfall statistics for all the rainfall thresholds throughout the integration duration compared to CNTL (figure 12). These results suggest that LDAS shows significant improvement (up to lead time of 72 hrs) in capturing the incident and moderate, medium and heavy to very heavy rainfall epochs (figures 11 and 12).

Further, the model predicted 24-hr accumulated rainfall at six different stations were compared with IMD ground based rain gauge observations (figure 13a–f). Those stations that received more than 250 mm of rainfall during 16–18 June (aggregate rainfall for 3 days) were selected for verification. It is noted that the LDAS rainfall for all the three days at all the stations are in good agreement with that of observed rainfall. Note that LDAS

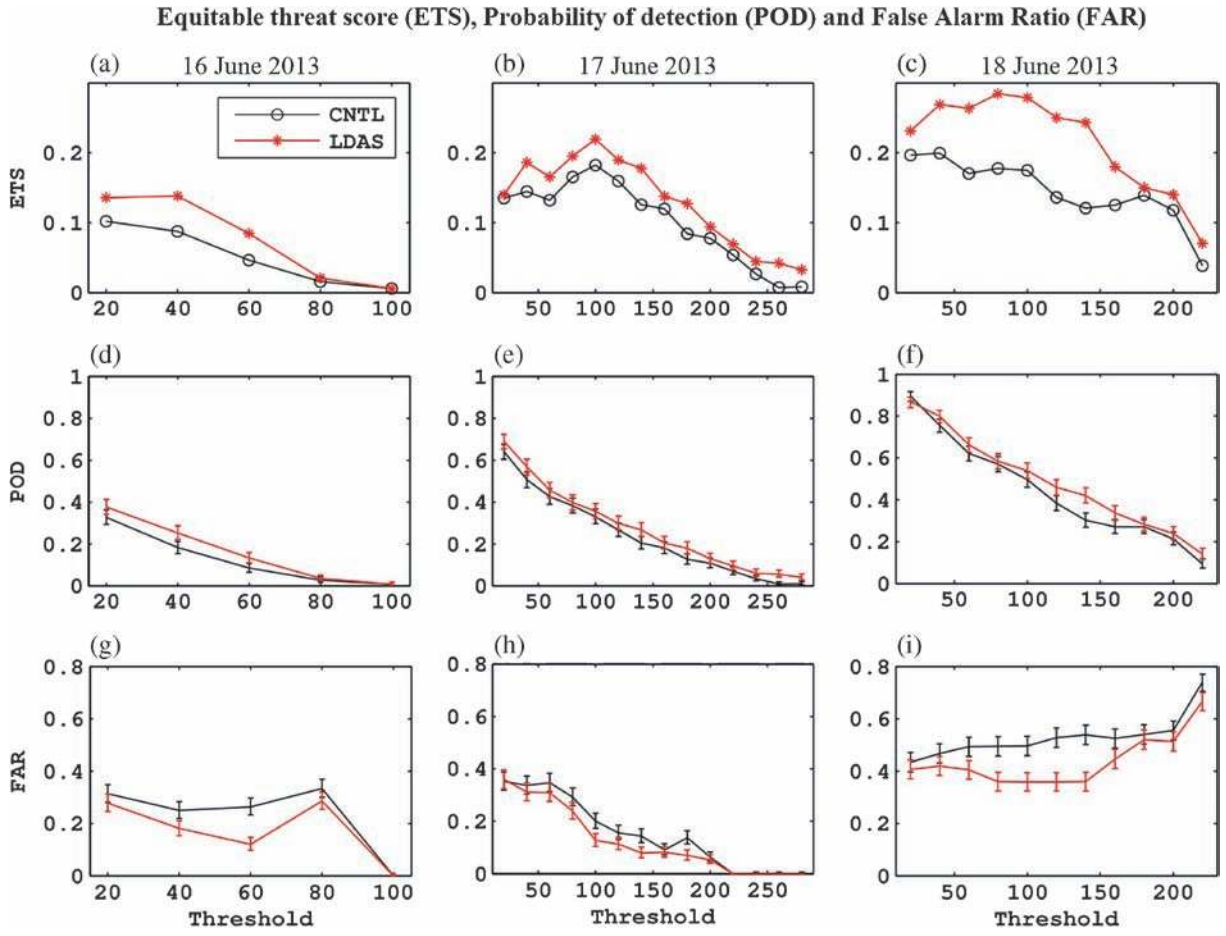

Figure 12. Equitable Threat Score (ETS), probability of detection (POD) and false alarm ratio (FAR) calculated at 95% confidence interval for daily accumulated rainfall for CNTL and LDAS validated with IMD daily data for (**a**, **d**, **g**) 16 June, (**b**, **e**, **h**) 17 June and (**c**, **f**, **i**) 18 June 2013.

showed slight higher rainfall amounts valid at 17 June 2013 with less error (∼17 mm) compared to CNTL rainfall. The 00 UTC 18 June rainfall for all these stations are remarkably well captured by LDAS compared to CNTL. Further, it is also found that there is no significant difference in area averaged (i.e., entire domain) daily accumulated rainfall between LDAS and CNTL. This highlights that although CNTL predicted the total rainfall in the affected region, it grossly misplaced the location (distribution), evolution and intensity, resulting in high errors in station-wise comparison. This analysis demonstrated the importance of high resolution land surface characteristic for improved prediction of moderate-to-heavy rainfall epochs.

Figure 14(a–c) shows the distribution of vertical velocity compared to WRF-3DVAR analysis for 1000–500 hPa over the heavy rainfall domain for 15–18 June 2013. It is noted that there is consistently higher vertical velocity cells over the LDAS domain and these updraft cells invigorate the convection, facilitating the heavy rainfall event. These results indicate that the vertical updraft cells are properly evolved in the LDAS compared to CNTL.

3.1.4 *Potential vorticity (PV)*

As the Uttarakhand rainfall event was rare of its kind due to the interactions of two different synoptic systems, in this subsection, PV analyses is discussed to analyse the interaction over the heavy rainfall region. Upper level PV intrusions over Indian region are generally accompanied by deep convection (Sandhya and Sridharan 2014). Figure 15(a–b) shows the temporal evolution of area averaged Ertel potential vorticity (PV) shaded and moisture convergence (contours) in the region of heavy rainfall from 12 UTC 14 June to 15 UTC 17 June. Peaks of large values of mid-level (300–700 mb) PV (>1 PV) is observed in the LDAS on 00 UTC 17 June and on 00 UTC of 18 June (figure 15b). It is noted that the moisture convergence maxima coincides with PV maxima, to

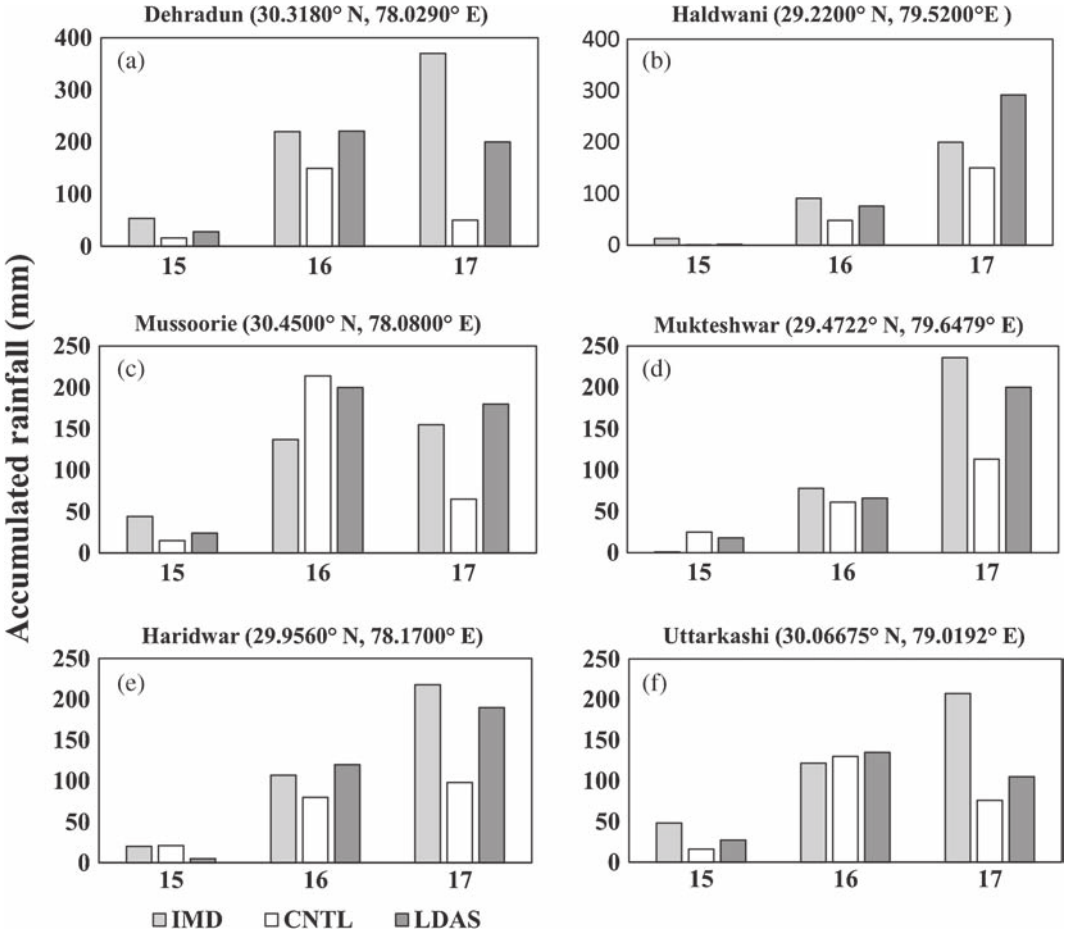

Figure 13. IMD rainfall (mm) verification of various stations that received heavy rainfall (>250 mm/3 day) validated with CNTL and LDAS simulated rainfall for 16, 17 and 18 June 2013. (**a**) Dehradun, (**b**) Haldwani, (**c**) Mussorie, (**d**) Mukteshwar, (**e**) Haridwar and (**f**) Uttarkashi.

suspect that the generation of PV contribution may be associated with the diabatic heating produced by latent heat release of the ascending moist air converging over this region associated with the stronger low level moisture availability (figure 6i). PV maxima for both the peaks at 00 UTC 17 and 18 UTC 17 are stronger than the CNTL (figure 13b). Huo *et al.* (1999) have expressed a method for partitioning the total PV perturbations to isolate distinct perturbations of different origins and to examine their interactions with each other and with the mean PV. According to them, the three major factors contributing the generation of PV are tropopause depression, surface baroclinicity, and latent heat release at lower troposphere. PV anomalies with relative humidity less than 30%, is mainly due to upper air contributions, whereas the PV perturbations associated with latent heat release have positive PV anomalies with greater than 70% relative humidity below 500 hPa.

Figure 16(a–f) shows the potential vorticity iso-surface (shaded with RH values) for six PVU anomalies within the study domain. The high PV anomalies that move eastward are having moderate RH (0–65%) values (figure 16a and b), suggest that these anomalies are the PV intrusions from upper tropospheric westerly trough valid for 00 UTC 16 June. We can recall from figure 1(a) that the northern limit of MD in LDAS is slightly ahead than CNTL during this time, and PV columns of LDAS with higher RH are distributed more towards the north (figure 16d). The interactions between the two synoptic scale systems is noted from 18 UTC 16 June onwards (within the circled region, figure 16d and f) and correspondingly large values of moisture convergence are found in LDAS (figure 15b). LDAS experiments show the persistence interaction of PV columns between westerly trough line and MD from 18 UTC 16 June to 09 UTC 17 June (not shown). And this persistent PV interaction have resulted in the stronger rainfall peak (figure 16b) in LDAS at 00 UTC 17 June. The advanced movement of PV columns in MD was due to relatively faster movement of the depression and can be attributed to the intensification of the low

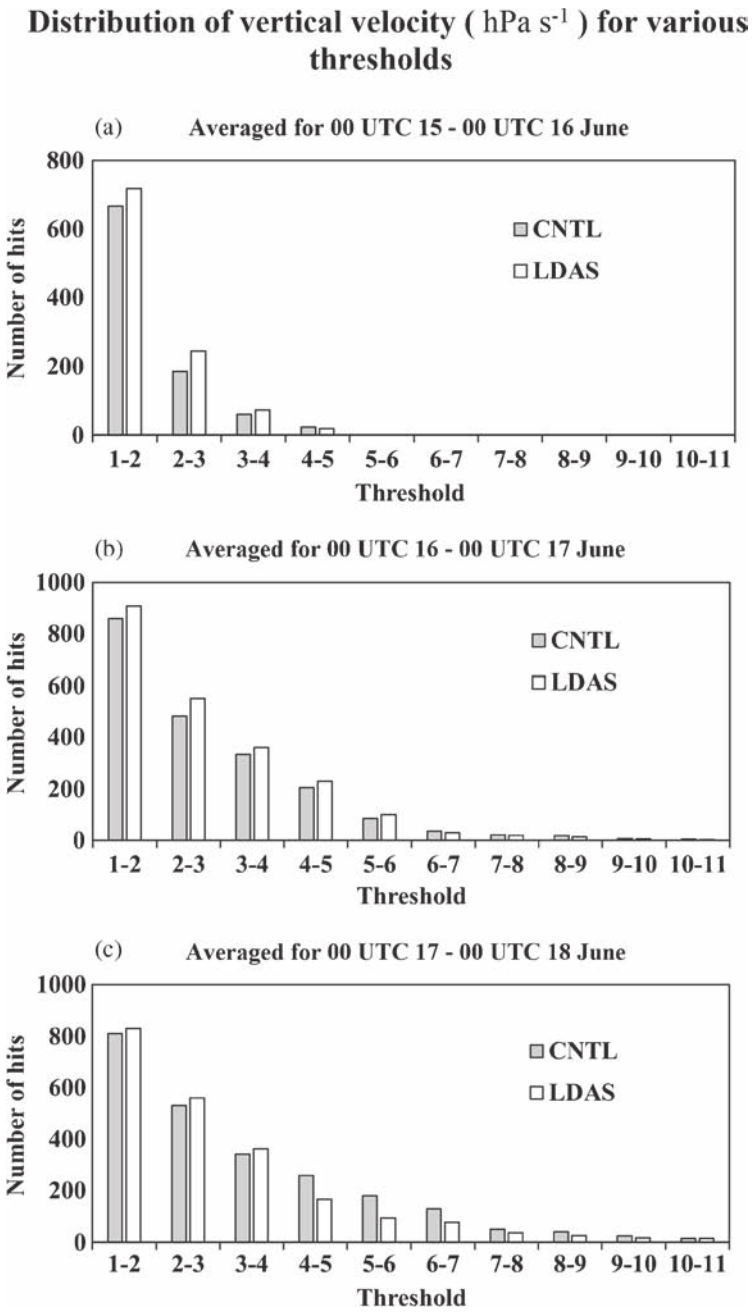

Figure 14. Validation of vertical velocity distribution (hPa s^{-1}) of various thresholds of vertical pressure velocity within the model grids compared with 3DVAR analysis within 1000–500 hPa layer for CNTL and LDAS averaged for 00 UTC (**a**) 15–16 June, (**b**) 16–17 June and (**c**) 17–18 June.

level convergence as noted in LDAS (figure 15b). Relatively stronger PV is noted at 18 UTC 17 June in the heavy rainfall region (figure 16f) and again during the second spell of intense rainfall occurred over the region (figure 15b).

The correlation coefficients between the area averaged surface rainfall and vertically averaged PV is 0.68 and 0.76, respectively for CNTL and LDAS, which fortifies the close relation between heavy rainfall and associated PV. Though experiments cannot segregate individual rainfall contributions from the westerly trough and MD, the actual contribution from the temporal evolution of PV advection and diabatic heating terms within the heavy rainfall region will be useful to understand how these two systems interacted. To see whether the increased PV generation in LDAS experiment is exclusively due to the merging of the two systems, contributions of advection and diabatic heating terms in the generation of PV is calculated for the heavy rainfall domain from simplified form of Ertel potential vorticity equation (Bluestein 1993) analysis. The quasi-static version of the Ertel PV tendency equation is expressed by:

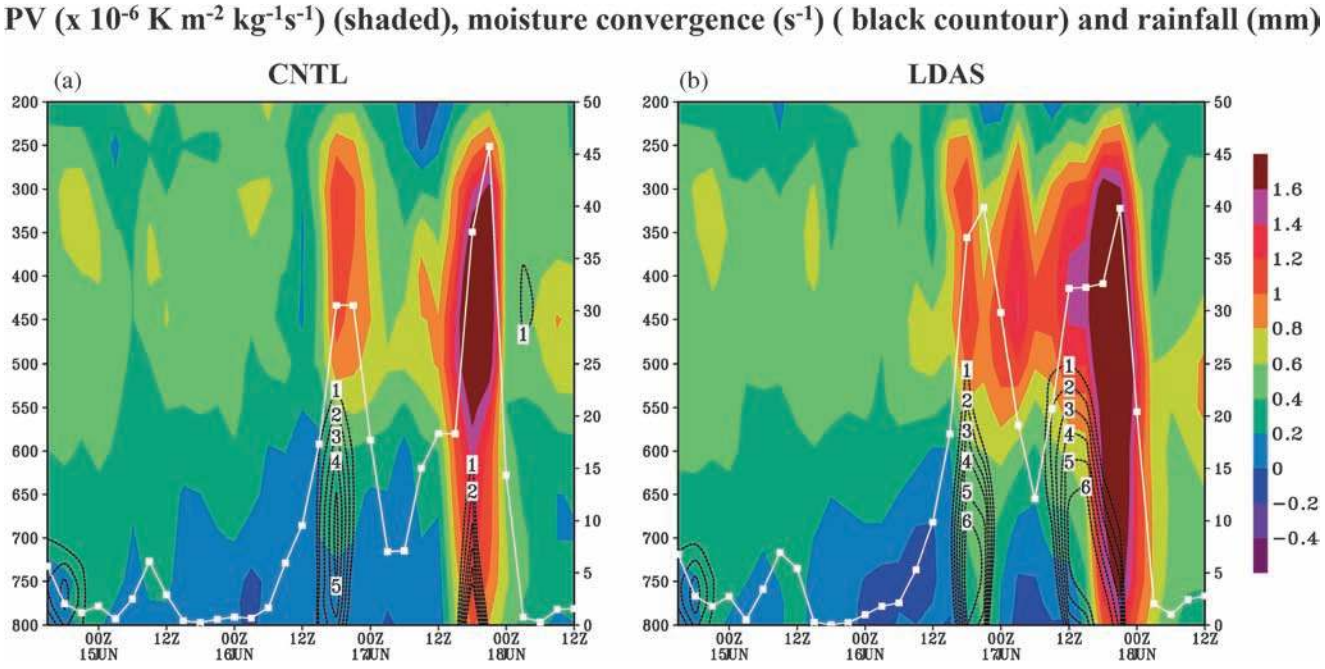

Figure 15. (**a**) Vertical structure of potential vorticity (shaded) ($\times 10^{-6}$ K m^{-2} kg^{-1}s^{-1}), moisture convergence (dashed contour) (s^{-1}) and associated rainfall (thick line) (mm) simulated by (**a**) CNTL and (**b**) LDAS.

$$\underset{\text{(I)}}{\frac{\partial}{\partial t}\left(-\zeta_{a\theta} g \frac{\partial \theta}{\partial \rho}\right)} = \underset{\text{(II)}}{\mathbf{V_H} \cdot \boldsymbol{\nabla}_\theta \left(-\zeta_{a\theta} g \frac{\partial \theta}{\partial \rho}\right)} - \underset{\text{(III)}}{\frac{d\theta}{dt}\frac{\partial}{\partial \theta}\left(-\zeta_{a\theta} g \frac{\partial \theta}{\partial \rho}\right)} + \underset{\text{(IV)}}{\left(-\zeta_{a\theta} g \frac{\partial \theta}{\partial \rho}\right)\frac{\partial}{\partial \theta}\frac{d\theta}{dt}} + \underset{\text{(V)}}{\left\{\boldsymbol{\nabla}\frac{d\theta}{dt} \cdot \frac{\partial (\mathbf{V}\times)_\theta}{\partial \theta}\right\} g \frac{\partial \theta}{\partial \rho}} - \underset{\text{(VI)}}{\left\{\boldsymbol{\nabla} \cdot (F\times)\right\}_g g \frac{\partial \theta}{\partial \rho}} \quad (1)$$

where term (I) represents local change in PV (generation term), term (II) is the horizontal advection of PV, term (III) is the vertical advection of PV, term (IV) represents vertical differential heating, term (V) is for horizontal differential heating and term (VI) represents the frictional term. The PV tendency terms are calculated for heavy rainfall domain along vertical only from 700–200 hPa considering to the terrain over the region. The results show vertical advection of PV is one order larger in magnitude than the other two heating terms and the sum of all the three heating terms will represent the total diabatic heating.

Figure 17(a, b) shows the local rate of change of PV for CNTL and LDAS, respectively. An increase in local change of PV is positive at two instances at between 12 UTC 16 and 00 UTC 17 June and 12 UTC to 15 UTC 17 June, respectively. These instances are well matched with the rainfall peaks as observed in figure 10(c). Horizontal advection of PV shows that, PV intrusions predominantly happened between upper and mid-levels (850–500 hPa) prior to the first spell of rainfall, which further extend to the surface levels (figure 17b, c). This could be the speculate as the first PV interaction between the two synoptic scale systems slightly after 12 UTC 16 June, having predominant contributions of PV associated with the westerly trough, as the intrusion is observed from upper levels, while MD position is still centered at 24.7°N–76.9°E for LDAS and 24.2°N–77.1°E for CNTL. LDAS PV advection seen from the lower to mid-levels for the same period (figure 17d), suggests that the close-by PV columns of MD started interacting with the PV columns induced by the westerly trough. The strong mid-level PV advection agrees well with the two rainfall maxima associated with the heavy rainfall centered over 00 UTC 17 and 18 UTC 17 June. At the same time, total diabatic heating have less contributions during the first spell of rainfall over the heavy rainfall domain, but have significant contributions during the second spell of rainfall. In LDAS, higher values of heating is noted at the lower levels at 00 UTC 17 June (figure 17e, f) which can be attributed to the more convectively unstable atmosphere (figure 10), high moisture convergence (figure 15b) and strong orographic lifting (figure 9d). This leads to the conclusion that the

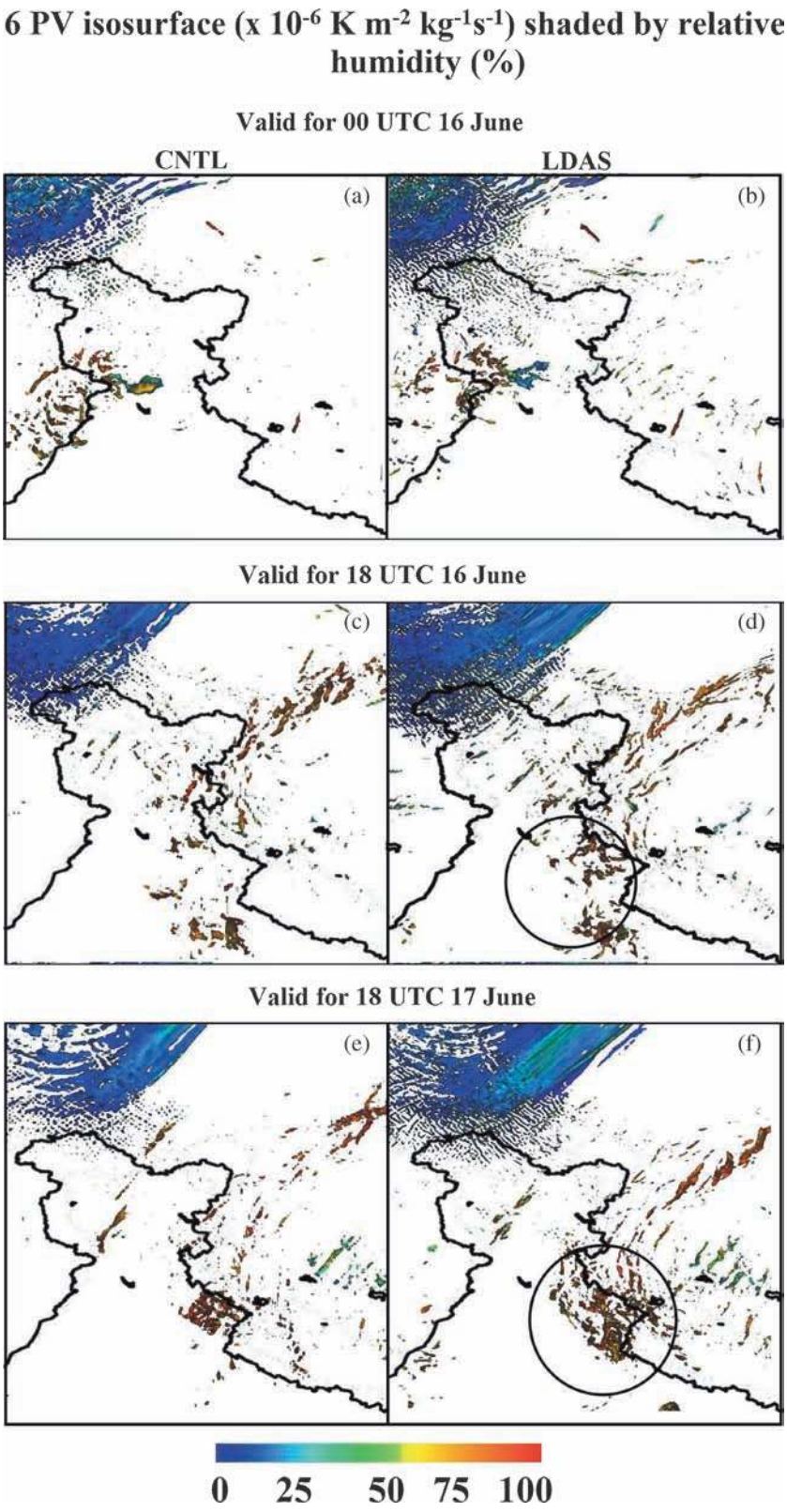

Figure 16. (**a**–**f**) Potential vorticity iso-surface of 6 PVU ($\times 10^{-6}$ K m^{-2} kg^{-1}s^{-1}) shaded by relative humidity (%) (**a** and **b**) at 00 UTC 16 June (**c** and **d**) at 18 UTC 16 June, (**e** and **f**) at 18 UTC 17 June 2013 for CNTL and LDAS, respectively. Wavy structure represents the high PV associated with upper tropospheric subtropical westerly, and cluster of loosely organized patches illustrate the lower to mid-level PV (high RH) associated with moving westerly trough and monsoon depression.

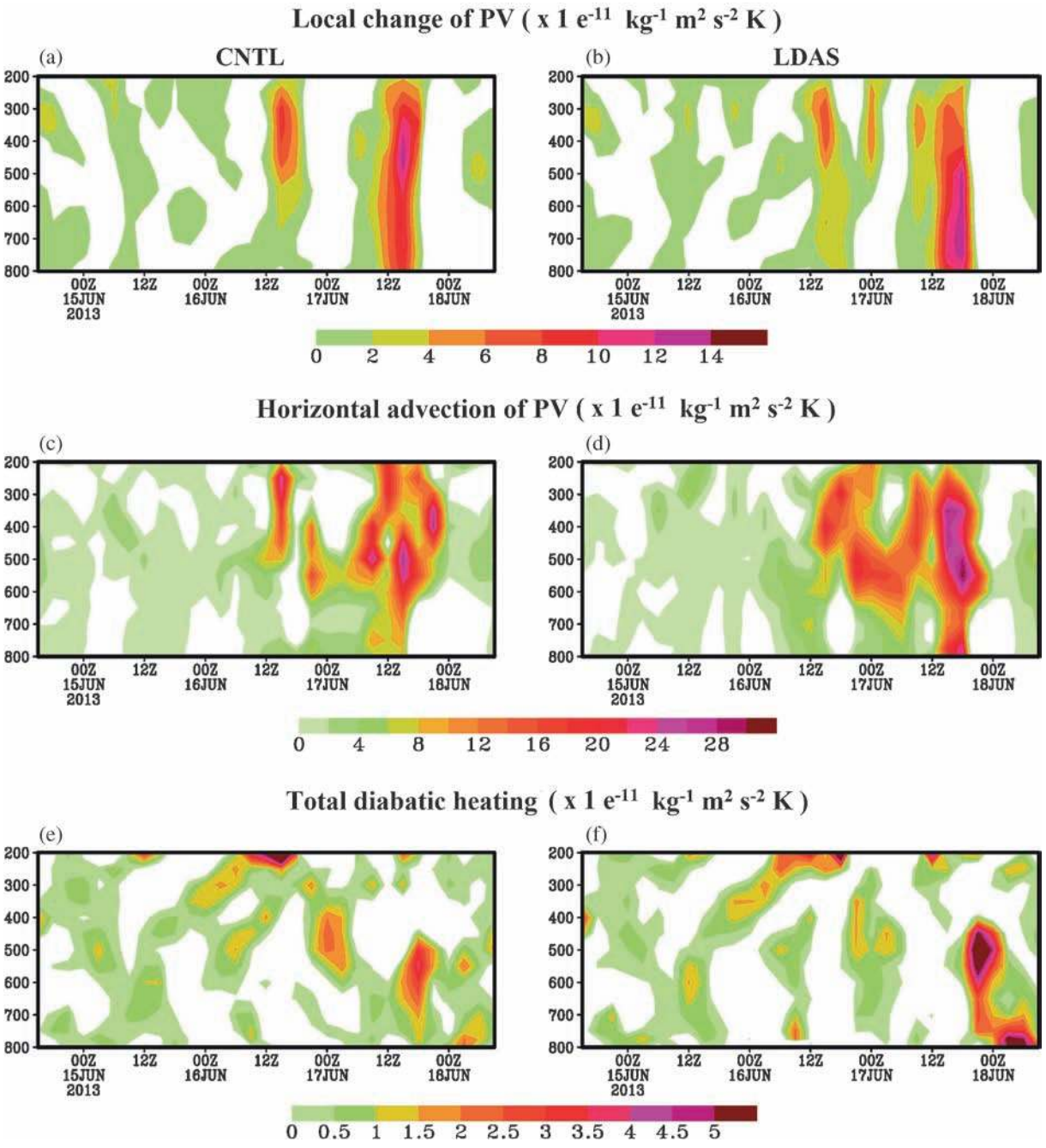

Figure 17. (**a**–**h**) Temporal evolution of potential vorticity terms in PV tendency equation calculated for the heavy rainfall region. (**a** and **b**) local rate of change of PV, (**c** and **d**) horizontal advection, (**e** and **f**) total diabatic heating terms, (**a**, **c**, **e**) CNTL, and (**b**, **d**, **f**) LDAS. Scale to e^{-10}.

generation of increased PV in LDAS is predominantly contributed by the advection of PV and the diabatic heating contribution associated with latent heat release due to the convergence of moisture to the total PV is considerably less. Further, it is clear that the advance progress of MD in LDAS experiment has led to the more realistic interaction in terms of magnitude and timing through PV columns, facilitating an increase in PV and rainfall over the region.

4. Summary

In this study, the role of land surface feedback in simulating the heavy rainfall event of Uttarakhand is investigated using WRF and HRLDAS modelling framework. This event was a result of multiple interactions of synoptic scale systems associated with the faster north westward propagation of monsoon depression supported by a stationary low pressure over west, which further interacted with

mid-latitude westerly trough. Soil moisture (SM) and soil temperature (ST) profiles are assimilated using HRLDAS for both inner (4 km) and outer (12 km), forcing for a period of 7 years with MERRA, TRMM and GLDAS and datasets for obtaining balance land state and injected into WRF model, initialized at 12 UTC 14 June 2013. Validation of HRLDAS, SM with IMD station observations yields better correlation and reduced RMSE error implies that LDAS experiment could reproduce point to point variability and provide superior initial lower boundary conditions in the model. Validation of the lowest layer temperature (T2) and specific humidity (Q2) with synoptic observations suggest that the LDAS experiment which utilizes the synthesized high resolution soil moisture and soil temperature fields as surface conditions in WRF model, has rendered more accurate evolution of the PBL characteristics than the CNTL. The heterogeneity in LDAS-based surface conditions created dry-wet soil discontinuity and help to produce conducive environment through the enhanced LH flux over central and north western parts of India, enabling intrusion of moisture from Arabian Sea deep into the sub-continental landmass. This is clearly evident from the anomalous cyclonic circulations (LDAS-CNTL) west of the Indian subcontinent. Temporal evolution of PV columns for both the experiments over the heavy rainfall region shows an increase in magnitude 6–12 hr prior to the event, but persistent values of higher PV associated with higher moisture convergence and rainfall in LDAS.

The rainfall result from both the experiment yields better correlation (∼0.7) with PV and moisture convergence. Increased CAPE with higher Lifted Index (LI) is seen by LDAS around 6–12 hr prior to the heavy rainfall episode centered at 00 UTC 17 June and strong PV columns are visible, coherent with enhanced moisture convergence and support increased orographic upliftment. These features are not well captured in CNTL run, in which coarser resolution soil moisture and soil temperature fields are interpolated and utilized as surface conditions. The LDAS is able to reproduce the observed two rainfall peaks with an error (∼17 mm), comparing to station-wise rainfall obtained from IMD, while, the same is about 60 mm in CNTL. It is also important to note that there was no significant difference between LDAS and CNTL, when area averaged 24-hr accumulated rainfall is considered. These results indicate that although CNTL predicted total rainfall (in the affected region) it misplaced the location (distribution), evolution and intensity of the rainfall. Further, the maximum impact on the rainfall skill is noted on 18 June 2013.

The realistic land surface conditions at model resolution in LDAS aid PV columns of MD which is modulated through surface turbulent fluxes due to positive soil moisture anomaly, lead to faster progress and interact with the PV columns of westerly trough in the vicinity of the affected region. LDAS experiment could well reproduce the evolution of synoptic systems, viz., westerly trough over North India, a low pressure area over the Arabian Sea and a depression in the Bay of Bengal and help improved rainfall prediction in terms of spatial distribution, amount and timing over Uttarakhand. The intrusion/generation of PV within the heavy rainfall domains have two contributors, viz., the upper air westerlies along the foothills of the Himalayan arc and the PV columns of the northerly moving MD over Uttarakhand region. To understand whether the increased PV generation in LDAS experiment is exclusively due to the interactions of the two systems, contributions due to the advection term is calculated employing simplified form of quassy static Ertel potential vorticity equation. Sum of three heating terms represents the total diabatic heating. It is realized that the PV advection term has contributed more to the total PV for the rainfall centered at 00 UTC 17, but a less but substantial contribution from the diabatic term for rainfall at 18 UTC 17 June. This leads to the conclusion that the generation of PV is predominantly contributed by the advection of PV and improved land state in LDAS has played a major role in triggering the interactions by accurate propagation and evolution of the cyclonic systems (i.e., cyclonic system over west and MD) through the accurate surface flux exchanges and further interactions with the westerly trough. The overall analyses of LDAS experiment demonstrate the importance of high resolution land surface characteristics for the prediction of moderate to heavy rainfall epochs, as seen in Uttarakhand event. Though a single event is studied in this paper, results are very robust and will be further extended to study other high impact weather systems.

Acknowledgements

The authors sincerely thank the anonymous reviewers for their valuable comments, which immensely helped to improve the quality of this manuscript. The authors are grateful for the Council of Science and Industrial Research (CSIR) award no. 09/1059(0005)/2013-EMR-I for supporting this work. Authors are also grateful to agencies namely, National Center for Environment Protection (NCEP) USA, Indian Meteorological Department (IMD) and National Aeronautics and

Space Administration (NASA) USA for providing datasets free of cost, to National Centre for Atmospheric Research (NCAR) for providing WRF and HRLADS modelling systems, Model Evaluation Tools (MET) and NASA's Grid Analysis and Display System (GrADS) graphic software that are open source models and softwares used in this study.

Appendix 1

The verification measures for categorical variables like ETS, POD, FAR and continuous variables like RMSE, correlation, mean error and multiplicative bias are carried out by means of Model Evaluation Tools (MET) statistical package. The statistics for categorical variables are formulated using the contingency table shown in table A1. In this table, f represents the forecasts and o represents the observations and the two possible forecast and observation values are represented by the values 0 and 1.

The values in table A1 are counts of the number of occurrences of the four possible combinations of forecasts and observations. The n_{ij} values in the table represent the counts in each forecast-observation category, where i represents the forecast and j represents the observations. The '.' symbols in the total cells represent sums across categories.

1) Equitable Threat Score (ETS)

ETS (also known as Gilbert Skill Score) is based on the Critical Success Index (CSI), corrected for the number of hits that would be expected by chance.

$$\mathrm{ETS} = \frac{n_{11} - C_1}{n_{11} + n_{10} + n_{01} - C_1}$$

$$C_1 = \frac{(n_{11} + n_{10}) \times (n_{11} + n_{01})}{T} = \frac{n_{1.} n_{.1}}{T}.$$

ETS values range from –1/3 to 1. A no-skill forecast would have ETS = 0; a perfect forecast would have ETS = 1.

$$\mathrm{CSI} = \frac{n_{11}}{n_{11} + n_{10} + n_{01}}$$

CSI is the ratio of the number of times the event $n_{11} + n_{10} + n_{01}$ was correctly forecasted to occur to the number of times it was either forecasted or occurred. CSI ignores the 'correct rejections' category (i.e., n_{00}). CSI is also known as the Threat Score (TS).

2) Probability of detection (POD)

POD is defined as:

$$\mathrm{POD} = \frac{n_{11}}{n_{11} + n_{01}} = \frac{n_{11}}{n_{.1}}.$$

It is the fraction of events that were correctly forecasted to occur and often known as hit rate. POD ranges from 0 to 1 and for a perfect forecast POD = 1.

3) False alarm ratio (FAR)

FAR is defined as:

$$\mathrm{FAR} = \frac{n_{10}}{n_{11} + n_{10}} = \frac{n_{10}}{n_{1.}}.$$

It is the proportion of forecasts of the event occurring for which the event did not occur. FAR ranges from 0 to 1 and FAR = 0 for a perfect forecast.

4) Root-mean-square error (RMSE)

RMSE is defined as the square root of Mean Square Error (MSE),

$$\mathrm{RMSE} = \sqrt{\mathrm{MSE}}$$

where MSE measures the average squared error of the forecasts

$$\mathrm{MSE} = \frac{1}{n} \sum_{i=1}^{n} (f_i - O_i)^2.$$

5) Correlation

Correlation measures the strength of linear association between observation and forecast. It is

Table A1. *Verification statistics.*

Forecast	Observation		Total
	$o = 1$ (e.g., Yes)	$o = 0$ (e.g., No)	
$f = 1$ (e.g., Yes)	n_{11}	n_{10}	$n_{1.} = n_{11} + n_{10}$
$f = 0$ (e.g., No)	n_{01}	n_{00}	$n_{0.} = n_{01} + n_{00}$
Total	$n_{.1} = n_{11} + n_{01}$	$n_{.0} = n_{10} + n_{00}$	$T = n_{11} + n_{10} + n_{01} + n_{00}$

defined as:

$$\text{Correlation} = \frac{\sum_{i=1}^{T}\left(f_i - \bar{f}\right)\left(O_i - \bar{O}\right)}{\sqrt{\sum\left(f_i - \bar{f}\right)^2}\sqrt{\sum\left(O_i - \bar{O}\right)^2}}$$

where $\bar{f}$ represents the forecast mean and $\bar{O}$ represents observation mean. Correlation varies between −1 and 1. Value of 1 indicates perfect correlation and value of –1 indicates perfect negative correlation. Value of 0 indicates that the forecasts and observations are not correlated.

6) Mean error

Mean error is a measure of overall bias for continuous variables and is the bias itself. It is defined as:

$$\text{ME} = \frac{1}{n}\sum_{i=1}^{n}\left(f_i - O_i\right).$$

7) Multiplicative bias

Multiplicative bias is the ratio of the means of forecast and observations and is defined as:

$$\text{MBIAS} = \frac{\bar{f}}{\bar{O}}.$$

References

Ashu Dastoor and Krishnamurti T N 1991 The landfall and structure of a tropical cyclone: The sensitivity of model predictions to soil moisture parameterizations; *Bound. Layer Meteorol.* **55** 345–380.

Boos W R, Hurley J V and Murthy V S 2014 Adiabatic westward drift of Indian monsoon depressions; *Quart. J. Roy. Meteorol. Soc.* **16** 1–16.

Bluestein H B 1993 Synoptic-dynamic meteorology in the mid latitudes; Volume II: Observations and theory of weather systems, Oxford University Press, New York, 594p.

Chand R and Singh C 2015 Movements of western disturbance and associated cloud convection; *J. Ind. Geophys. Union* **19(1)** 62–70.

Chang Hsin I, Niyogi D, Kumar A, Kishtawal C M, Dudhia J, Chen F, Mohanty U C and Shepard M 2009 Possible relation between land surface feedback and the post-landfall structure of monsoon depressions; *Geophys. Res. Lett.* **36(15)** 15826.

Chen F, Kevin W Manning, Margaret A LeMone, Stanley B Trier, Joseph G Alfieri, Rita Roberts, Mukul Tewari, Dev Niyogi, Thomas W Horst, Steven P Oncley, Jeffrey B Basara, Peter D Blanken and Chen Fei 2007 Description and evaluation of the characteristics of the NCAR high-resolution land data assimilation system; *J. Appl. Meteorol. Climatol.* **46(6)** 694–713.

Das P K 1968 The Monsoon; National Book Trust, New Delhi, India.

Done J, Davis C and Weisman M L 2004 The next generation of NWP: Explicit forecasts of convection using the weather research and forecasting (WRF) model; *Atmos. Sci. Lett.* **5** 110–117.

Ek M B 2003 Implementation of Noah land surface model advances in the National Centers for Environmental Prediction Operational Mesoscale Eta Model; *J. Geophys. Res.* **108** (D22).

Guillod B P, Orlowsky B, Miralles D G, Teuling A J and Seneviratne S 2015 Reconciling spatial and temporal soil moisture effects on afternoon rainfall; *Nat. Commun.* **6** 6443.

Hara M, Kimura F and Yasunari T 2004 The generation mechanism of the western disturbances over the Himalayas; The 6th International Study Conference on GEWEX in Asia and GAME, GAME CD-ROM Publ. 11, Abstract T4HM09Aug04145134; *World Clim. Res. Programme*, Geneva, Switzerland.

Holt T R, Niyogi D, Chen K, Manning M, Lemone A and Qureshi A 2005 Effect of land–atmosphere interactions on the IHOP 24–25 May 2002 Convection Case; *Mon. Wea. Rev.* **134** 113–133.

Hong S-Y and Lim J-O J 2006 The WRF single-moment 6-class microphysics scheme; *J. Korean Meteor. Soc.* **42** 129–151.

Hong S-Y, Noh Y and Dudhia J 2006 A new vertical diffusion package with an explicit treatment of entrainment processes; *Mon. Wea. Rev.* **134** 2318–2341.

Huffman George J, David T Bolvin, Eric J Nelkin, David B Wolff, Robert F Adler, Guojun Gu, Yang Hong, Kenneth P Bowman and Erich F Stocker 2007 The TRMM Multisatellite Precipitation Analysis (TMPA): Quasi-global, multiyear, combined-sensor precipitation estimates at fine scales; *J. Hydrometeor.* **8** 38–55.

Huo Zonghuai, Zhang D L and Gyakum J R 1999 Interactions of potential vorticity anomalies in extratropical cyclogenesis; Part I, Static Piecewise Inversion, **127** 2546–2561.

India Meteorological Department (IMD) July 2013 A preliminary report on heavy rainfall over Uttarakhand during 16–18 June 2013.

Kain J S 2004 The Kain–Fritsch convective parameterization: An update; *J. Appl. Meteor.* **43** 170–181.

Kishtawal C M, Dev Niyogi, Mukul Tewari, Roger A Pielke and Marshall Shepherd J 2010 Urbanization signature in the observed heavy rainfall climatology over India; *Int. J. Climatol.* **30(13)** 1908–1916.

Koster Randal D *et al.* 2004 Regions of strong coupling between soil moisture and precipitation; *Science* **305(5687)** 1138–1140.

Kotal S D, Soma Sen Roy and Roy Bhowmik S K 2014 Catastrophic heavy rainfall episode over Uttarakhand during 16–18 June 2013 – Observational aspects; *Curr. Sci.* **107(2)** 234–245.

Lei M, Niyogi D, Kishtawal C, Pielke Sr. R, Beltrán-Przekurat A, Nobis T and Vaidya S 2008 Effect of explicit urban land surface representation on the simulation of the 26 July 2005 heavy rain event over Mumbai, India; *Atmos. Chem. Phys.* **8** 5975–5995.

Mitra A K, Monin I M, Rajagopal E N, Basu S, Rajeevan M N and Krishnamurti T N 2013 Gridded daily Indian monsoon rainfall for 14 seasons: Merged TRMM and IMD gauge analyzed values; *J. Earth Syst. Sci.* **122** 1173–1182.

Mooley D A 1957 The role of western disturbances in the production of weather over India during different seasons; *Ind. J. Meteor. Geophys.* **8** 253–260.

Pal Jeremy S, Elfatih A and Eltahir B 2003 A feedback mechanism between soil-moisture distribution and storm tracks; *Quart. J. Roy. Meteorol. Soc.* **129(592)** 2297.

Pisharoty P R and Desai B N 1956 Western disturbances and Indian weather; *Ind. J. Meteorol. Geophys.* **8** 333–338.

Saha Subodh K, Halder S, Krishna Kumar K and Goswami B N 2011 Pre-onset land surface processes and 'Internal' interannual variabilities of the Indian Summer Monsoon; *Clim. Dyn.* **36(11–12)** 2077–2089.

Sandhya M and Sridharan S 2014 Observational relations between potential vorticity intrusions and pre-monsoon rainfall over Indian sector; *Atmos. Res.* **137** 80–90, doi: 10.1016/j.atmosres.2013.09.013.

Skamarock W C, Klemp Joseph B, Dudhia Jimy, Gill David O, Barker Dale M, Wang Wei and Jordan G Powers 2008 A description of the advanced research WRF Version 3. NCAR/TN-468+STR, NCAR Technical Note Mesoscale and Microscale Meteorology Division, National Center for Atmospheric Research, Boulder, Colorado, USA.

Trier S B, Chen F and Manning K W 2004 A study of convection initiation in a mesoscale model using high resolution land surface initial conditions; *Mon. Wea. Rev.* **132** 2954–2976.

Vinodkumar A, Chandrasekar K Alapaty and Dev Niyogi 2008 The impacts of indirect soil moisture assimilation and direct surface temperature and humidity assimilation on a mesoscale model simulation of an Indian monsoon depression; *J. Appl. Meteorol. Climatol.* **47(5)** 1393–1412.

Yoon J H and Huang W R 2012 02 Indian monsoon depression: Climatology and variability; Modern Climatology, Book.

Zhang D and Anthes R A 1982 A high-resolution model of the planetary boundary layer – Sensitivity tests and comparisons with SESAME-79 Data; *J. Appl. Meteor.* **21** 1594–1609.

MS received 29 June 2015; revised 6 October 2015; accepted 24 November 2015